A STUDY OF APPLYING PARA RUBBER SHEETS IN RAILWAY TRACK BY USING BALLAST BOX TEST

Mr. Somkith Dethvongsone

การศึกษาการใช้ยางพาราแผ่นในทางรถไฟด้วยการทดสอบกล่องหินโรยทาง

นายสมคิต เดชวงษ์สอน

Thesis Title	A STUDY OF APPLYING PARA RUBBER SHEETS IN RAILWAY TRACK BY USING BALLAST BOX TEST
By	Mr. Somkith Dethvongsone
Field of Study	Civil Engineering
Thesis Advisor	Assistant Professor Boonchai Sangpetngam, Ph.D.

Accepted by the Faculty of Engineering, Chulalongkorn University in Partial Fulfillment of the Requirement for the Master of Engineering

.... Dean of the Faculty of Engineering
(Associate Professor Supot Teachavorasinskun, D.Eng.)

THESIS COMMITTEE

.... Chairman
(Associate Professor Kasem Choocharukul, Ph.D.)
.... Thesis Advisor
(Assistant Professor Boonchai Sangpetngam, Ph.D.)
.... Examiner
(Associate Professor MANOJ LOHATEPANONT, Ph.D.)
.... External Examiner
(Athaphon Kawprasert, Ph.D.)

จุฬาลงกรณ์มหาวิทยาลัย
CHULALONGKORN UNIVERSITY

สมคิด เดชวงษ์สอน : การศึกษาการใช้ยางพาราแผ่นในทางรถไฟด้วยการทดสอบ
กล่องหินโรยทาง. (A STUDY OF APPLYING PARA
RUBBER SHEETS IN RAILWAY TRACK BY
USING BALLAST BOX TEST) อ.ที่ปรึกษาหลัก : ผศ. ดร.บุญชัย
แสงเพชรงาม

เมื่อไม่นานมานี้ ความพยายามที่จะลดการสึกหรอของหินโรยทางรถไฟ กลายเป็นประเด็นหลักสำหรับงานรถไฟ และงานวิจัยต่างๆ การสึกหรอของหินก่อให้เกิดการทรุดตัวของทางรถไฟและนำไปสู่ค่าบำรุงรักษาที่สูงในการซ่อมแซมรูปทรง ของรางรถไฟและในการทำความสะอาดหินปัจจุบันมีการพิสูจน์ที่ประสบความสำเร็จแล้วว่าการใช้แผ่นยางสังเคราะห์ที่มีความ ยืดหยุ่นรองใต้หมอนรถไฟและแผ่นรองใต้หินโรยทางรถไฟสามารถลดการสึกหรอของหินและการสั่นสะเทือนได้ยางพาราเป็น วัสดุธรรมชาติที่มีความยืดหยุ่นและมีจำนวนมากในภูมิภาคเอเชียตะวันออกเฉียงใต้ ดังนั้นงานวิจัยนี้จึงมีวัตถุประสงค์เพื่อศึกษา การใช้ยางพาราเป็นวัสดุทางเลือกของการลดการสึกหรอของหินโรยทางรถไฟ โดยได้ทำการทดลองเพื่อศึกษาพฤติกรรมการสึก หรอของหิน การทรุดตัวและโมดูลัสการคืนตัวของวัสดุในกล่องภายใต้สภาพการของโหลดที่เหมือนกันกัน ในการศึกษานี้ได้มี การจำลองแรงจากน้ำหนักเพลารถไฟที่ 20 ตันโดยจำลองสภาพที่รถวิ่งบนโครงสร้างที่มีหินโรยทางนั้นอยู่พื้นแข็งโดยใช้ กล่องหินจำลองโครงสร้างทางในการตรวจสอบการใช้ยางพาราเป็นแผ่นรองใต้หมอนและเป็นแผ่นรองใต้หินโรยทาง นอกจากนี้ ก่อนและหลังการทดสอบได้มีการใช้การประมวลผลภาพเพื่อวัดขนาดของหินทุกก้อนที่ทำการทดสอบ ผลการศึกษาพบว่าแผ่น รองใต้หมอนที่ทำจากยางพาราสามารถลดปริมาณการแตกของหินได้ถึง 80% เทียบกับตัวอย่างหินที่ไม่ใส่อะไรเลย นอกจากนี้ แนวโน้มของการทรุดตัวและโมดูลัสของคืนตัวของวัสดุในกล่องใกล้เคียงกับตัวอย่างอ้างอิงมากที่สุด จึงสรุปได้ว่าการศึกษานี้ ชี้ให้เห็นว่าศักยภาพในการใช้ยางพารายในรูปแบบแผ่นรองใต้หมอนควรนำมาใช้ในทางรถไฟ.

จุฬาลงกรณ์มหาวิทยาลัย
CHULALONGKORN UNIVERSITY

สาขาวิชา	วิศวกรรมโยธา	ลายมือชื่อนิสิต	
		....	
ปีการศึกษา	2561	ลายมือชื่อ อ.ที่ปรึกษาหลัก	
		....	

Somkith Dethvongsone : A STUDY OF APPLYING PARA RUBBER SHEETS IN RAILWAY TRACK BY USING BALLAST BOX TEST. Advisor: Asst. Prof. Boonchai Sangpetngam, Ph.D.

Recently, attempts to reduce ballast degradation have been a major topic for many railways and researchers. Nowadays, a successfully proven alternative is applied elastic under-sleeper pads in between sleeper and ballast particles, and also as the ballast mat placed under the ballast layer. The using of synthetic material as the elastic element is able to decrease the deterioration of ballast and vibrations. Para rubber is a natural elastic material and it is abundant in South East Asia countries. Therefore, this study is aimed to investigate using para rubber as an alternative element of reducing ballast breakage in ballasted track. Experiments were conducted to study ballast behaviors namely the particle breakage, deformation, and modulus of box reaction under similar loading conditions. In this study, cyclic loads from the train at axle loads of 20 tons were simulated on the rigid foundation condition using ballast box to investigate the use of para rubber as an under sleeper pad and ballast mat. Besides, before and after the tested ballast with the elastic element, the application of image processing was used to measure the dimensions of ballast particles to measure the size of particles. Results reveal that the under-sleeper pad made of para rubber can reduce the amount of ballast breakage by 80% of pure ballast case. In addition, the trend of settlement and modulus of box reaction are closed to the ballast reference the most. So In conclusion, this study indicates that the potential of using para-rubber under sleeper pads shall be considered in railway track.

จุฬาลงกรณ์มหาวิทยาลัย
CHULALONGKORN UNIVERSITY

Field of Study:	Civil Engineering	Student's Signature	....
Academic Year:	2018	Advisor's Signature	....

ACKNOWLEDGEMENTS

TABLE OF CONTENTS

LIST OF TABLES

LIST OF FIGURES

จุฬาลงกรณ์มหาวิทยาลัย
CHULALONGKORN UNIVERSITY

CHAPTER 1
INTRODUCTION

1.1 Background

Numerous countries around the world use railway transportation as one important mode to transport passengers and freight. The rapid growth of economy and population, as well as growing traffic in highway transport and a icreasing demand for fuel as a result of applying heavier and faster railway to provide passenger service, and to achieve efficient and cost-effective service in rail industries. To support higher service and to increase traffic of locomotives on the rail track, the ballasted track which is the primary use in railway system must be improved. Especially the ballast layer that is the first part of substructure element in rail track foundation have to serve as a bed for rail track and provides stability for the substructure while the train is moving and distribute the load. Similarly, it offers better water flowing and inhibits the growth of vegetation that might block track operation. An increment of passage traffic rise the dynamic load. The ballast particles were degrade by heavy load which cause the track settlement and track irregularities, track elements damaged, and more frequent track maintenance (Indraratna et al., 2011; Selig and Waters, 1994). In order to provide effective service and safety, the ballast tamping and surface alignment have to be used. In railway industry, minimizing the ballast degradation is essential, not only increase the ability to support heavier traffic, but it can reduce maintenance cost and increase life service of the railway system.

The critical area which has high track modulus mostly located at the bridge, tunnels, elevated station, track crossing, switches and grade separation. The speed restriction, stoppages, and delays frequently happen if this localizes area was maintained and repairs. So numerous research studies have been undertaken to quantify the benefit of using the resilient material as reinforcing or attach in a track bed structure. The resilient material use in rail track has been placed in three interfaces: rail pat attached at the rail-sleeper interface, under sleeper pads- attach under sleeper at the sleeper-ballast interface, ballast mat place on concrete or rigid interface in the case of bridge or tunnels. The solution of resilient material is to reduce degradation of ballast such as the studied from overseas found that the use of ballast mat can reduce the vibration to the granular layer, the soft surface ability can increase track geometry stability and ballast compression on the rigid substructures such as bridge or tunnels (Getzner, 2015). In addition, there is the use of polyurethane adding to the ballast to filling the voids between particle which possible to reduce permanent track settlement (Kennedy, 2011). In the same way, there are studies focus on using crumb rubber (tire cut in small piece) to reduce ballast deterioration by mixture with ballast and tire aggregate bound together with a resilient epoxy binder. Another

project studied the influence of crumb rubber to ballast by adding it in percentage without binder material in the laboratory.

The study form oversea has the better solution on using resilient material reinforcing ballast. Moreover, there are not many studies in Thailand about using the resilient material to improve ballast aggregate. Most of the resilient material is made from Para rubber. The Para rubber is made from the latex mixture with Acid through processing that rubber grower can produce by themselves. Beside that Para-rubber is a perennial plant known as the essential economic crop of Thailand but now it is facing the price depression situation, and the government is trying to solve that problem by supporting the usage of Para rubber in the country.

So that the application of Para rubber added to ballast particle to improve ballast behavior due to the elastic properties of rubber will be focused in this research. To reduce ballast deterioration, para rubber is available that can be used to undertake various function within the substructure of rail track, to ultimately increase track resistance degradation and to decrease deformation of railway track.

1.2 Objectives

The principal objectives of this study are:
1. Investigation of the ballast particle shape deterioration under repeated load application in the laboratory scale using a box test.
2. Study the potential use of Para rubber for reducing ballast deterioration.
3. Study between alternatives of applying Para rubber into ballast formation

1.3 Scope of Research

As mention at first the aim of this study is Para rubber as a mixture of railway ballast to improve its behavior on stabilizing the rail track alignment so that the scope of this study are:
1. Use ballast aggregate with the gradation used in State Railway of Thailand (SRT) railway construction.
2. The study uses laboratory test setup to simulate the ballast deterioration at a condition where ballast is placed on concrete or steel structure directly without any sub-ballast or soil foundation.

1.4 Expected Output

1. To verify the potential of applying Para rubber in ballast on deterioration resistance.
2. To obtain the best alternatives of applying Para rubber into ballast formation.

1.5 Thesis Outline

The procedure of this thesis starts from the literature review on related works, a brief overview of railway track behavior and components are presented. The substructure problems are also described by an explanation of other research and result. The different methods that use to improve ballast quality and reduce the required maintenance. Another ballast testing and its behavior were discussed. Then there is design and construct the tools for test, preliminary examination of the experimental arrangement, using instrument and investigate the materials used to this study. Later all component that will be used for testing was prepared, the ballast texture sample has to be recorded before and after testing on the box. While examining the data rocker and other devices attached to the samples also record the data. After finish testing, the data from recorder are then analyzed to determine any meaning.

```
┌─────────────────────────────────────┐
│   Literature and research review    │
└─────────────────────────────────────┘
                  │
                  ▼
┌─────────────────────────────────────┐
│ Design and preparing material/device testing │
└─────────────────────────────────────┘
                  │
                  ▼
┌─────────────────────────────────────┐
│  Proceed testing                    │
│  - Basic testing of aggregate       │
│  - Prepare and install the sample   │
│  - Image processing analysis        │
│  - Repeated load testing            │
└─────────────────────────────────────┘
                  │
                  ▼
        ┌──────────────────┐
        │     Analysis     │
        └──────────────────┘
                  │
                  ▼
        ┌──────────────────┐
        │   Conclusion     │
        └──────────────────┘
```
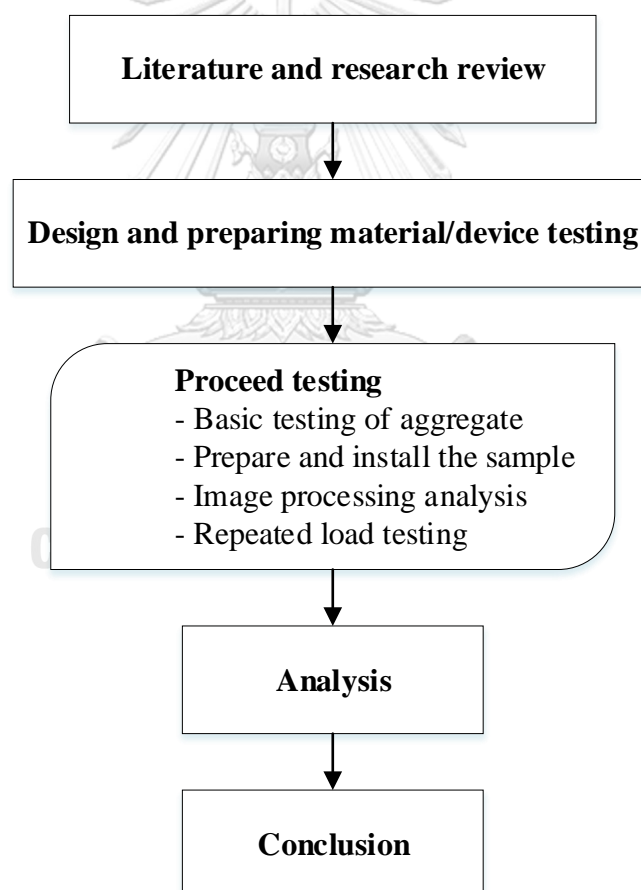
Figure 1.1 Test planning

CHAPTER 2
LITERATURE REVIEW

2.1 Ballast
2.1.1 Definition

The crushed aggregated that was used in railway is called "Ballast", it is located on the upper side of the sub-ballast layer to support the superstructure and to stabilize the rail track to transfer the high load capacity of the train through the underground. Because of the lower cost for railway construction, this rock is still a favorite substance in many countries. However, the most suitable quality of crushed material that can provide the best railway performance has to be hard, have similar gradations, easy to keep clean or re-clean, feasible and resistant to deformation under heavy traffic load.

2.1.2 Functions of ballast in railway track

According to the study of track substructure components (Selig and Waters, 1994), ballast has several functions:
- Support the superstructure uniformly with high bearing capacity by providing a firm and stable platform.
- Stabilize the sleeper when the forces (vertical, longitudinal, and lateral force) generated from train movement against to sleeper.
- Reduce high pressures from the underneath sleeper area to the subgrade layer at an acceptable level.
- Provide suitable drainage void for the track.
- Provide the resilience of the material to absorb energy when the material is deformed elastically.
- Reduce growth of plants.
- Facilitate track maintenance to be comfortable.
- Provide enough voids to reduce the dust storage.
- Absorb noise.
- Preventing and reducing the escape of electricity from street-railway.

2.1.3 Source of Ballast Rock

Ballast is usually composed of crushed rocks originating from hard stone. The source of ballast used in railway track of any country depends on the quality and availability of stone, and economy. There are no worldwide characteristic specification of ballast for its size, shape, abrasion resistance and mineral composition (Salim, 2004), therefore, the ballast have to have many types around the world. The ballast that Thailand railway required should be a kind of stone such as Granite,

Basalt, Rhyolite, Andesite, Quartzite, Dacite, Diorite, and Gabbro. The material should be an angular shape with the flakiness and elongation index not over 30% which was tested to be in accordance to BS 812 standard. Moreover, the percentage of deterioration should not exceed 25% when the test on Los Angeles Abrasion follows the standard ASTM C535. The aggregate is composed of medium size to large gravel sized around 20-60mm.

2.2 Effects of Ballast Degradation
2.2.1 Fouling

(Indraratna et al., 2011) expressed that fouling on the railway occurred by many reasons such as breakage of ballast, clay in sub-ballast pumping up to the ballast layer, dust for wind blowing (rail track on the desert), spillage from freight traffic and during construction. Selig and Waters, (1994), described that when fouling is storage in the ballast layer, it will cause the increasing of the shear strength and stiffness. In contrast, when the fouling is faced with water, it would increase the ballast deterioration and the rate of the settlement will also rise up. The smaller piece of railway aggregates usually rises the track settlement which can decrease the resistance angle, and even cause variance settlement which can lead to the unsterilized of track alignment. Therefore, the fouling must be cleaned by water or replaced by new aggregate to maintain the desired track stiffness (resiliency), bearing capacity, and level of safety. There is a use of elastic material mixed into the ballast to reduce aggregate breakages such as automobile tire-derived aggregate or crumb rubber to prevent fouling. Besides that, the use of geotextile is placed between the ballast layer and sub-ballast in order to filter the sub-ballast pumping up to ballast.

Figure 2.1 Fouling of ballast (Indraratna et al., 2011)

2.2.2 Drainage

The breakage of material downward to fill the void space in ballast causes the reduction of drainage ability of ballast layer (Indraratna et al., 2011). The pore water unable to flow to drainage can reduce the friction between aggregates and loss of its stiffness and also resiliency. The mixing between ballast and fouling in wet condition minimize track stability and continues the deterioration of track components later. (Kashani et al., 2017) studied the behavior of ballast aggregate at water content conditions and found that the highly fouling at saturating condition increased twice of the settlement in comparison with the field condition.

Figure 2.2 Ponding water in ballast layer (Indraratna et al., 2011)

2.2.3 Deformation

The ballast deformation occurred by the compaction of ballast and the particle breakages. According to (Selig and Waters, 1994), it has been stated that the changing railway alignment along the length of the track is not significant than the differential track deformation. However, rather than the distortion on subgrade, the ballast deformations still have various ways to solve its failure without disturbing the operation. (Kashani et al., 2017; Indraratna et al., 2006; Raymond, 2002) according to their experimental studies, it was found that the trainload influences the ballast layer deformation, the number of load cycles, and speed of the train. Moreover, the type of ballast, reinforcement material , particle size distribution, and rate of saturating are the factor effects of differential deformation of aggregates.

Figure 2.3 Differential settlement in rail track caused from the deformation of ballast (Indraratna et al., 2011).

(Salim, 2004) suggested that the track geometry maintenance effected from the growing of traffic cover of three froms: Tamping is the maintenance work which used to return the position of railway structure. This method is quite a popular used for maintenance activities on railway track although it is the one factor which causes the ballast degradations and generates stone dust (Selig and Waters, 1994).
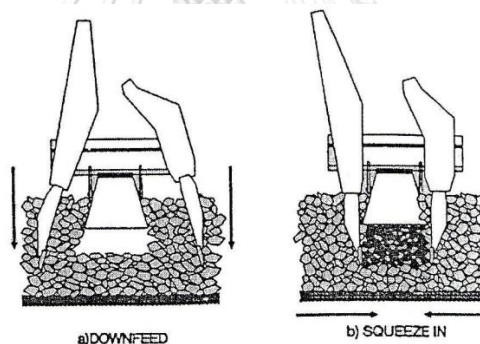
Figure 2.4 Tamping maintenance (Selig and Waters, 1994)

On the other hand, there is a stone blowing machine which is the maintenance method to minimized disturbance of ballast under sleeper because it lifts the superstructure up in light position and blows small aggregate beneath the void between crushed rock and tie. A particular laboratory uses ballast box to simulate loading condition to compare different material and maintenance (tamping and stone-blowing). They showed that stone-blowing could improve the track performance significantly (D'Angelo et al., 2015).
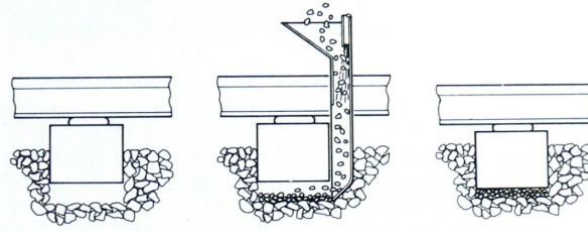
Figure 2.5 Stone-blowing maintenance (Selig and Waters, 1994)

Ballast cleaning and renewal is the method that uses when the ballast gets excessively fouled, but the railway track still deformed even using tamping or stone-blowing, in this case, ballast must be cleaned or changed by the new aggregate. Ballast layer maintaining process are costly and consume more time; furthermore, it disturbs train operating, so this process is not often undertaken.

2.2.4 Track lateral movement

This failure occurred when the ballast degraded and when there is a lack of lateral restriction to maintain rail stability. The misalignment of the rail happens on both direct and curve way making the lateral ballast restriction reduced causing the flowing down along slopes. (Zakeri, 2012) mentioned that the track lateral movement is influence by sleeper type, weight, dimension of sleeper, ballast gradation, ballast stone quality, ballast depth in the crib and the shoulder height from the bottom of sleeper, ballast compaction, rail and fasteners type. At the same time, he also said that the significant affect that impacted the total lateral resistance of sleeper is the side frictional resistance, the bottom resistance of sleeper, and the end resistance. Moreover, the track lateral movement occurred when the steel rail faced with high thermal because it overcomes the lateral resistance of sleeper. There are several methods to increase the lateral resistance of sleeper and ballast such as winged sleeper, frictional sleeper and large sleeper (Koike et al., 2014). (Zakeri, 2012) Did the field test of lateral resistance of rail track found that the use of the frictional concrete sleeper can increase the lateral resistance by 67%. So the reason learning from this is that the lateral confinement not only effects from the ballast but friction from sleeper is also one factor reducing lateral movement of rail.

Figure 2.6 Track buckles because of lacking lateral confinement
(Indraratna et al., 2011)

2.2.5. Track modulus

Track failure is a major issue in many railroad accidents. Track modulus, or stiffness, is an essential parameter in track quality. Track modulus is definite as the supporting force divided by unit length of rail per unit deflection and can be used as a record of railway performance. The optimum value for track modulus should not be too high or too low. Too high value (too stiff) would lead to fatigue, fracture and excessive vibrations. An excessively low track modulus value would cause unwarranted deformations and even permanent deformation (Selig and Waters, 1994). There are many factors influence track modulus such as the quality of rails, sleepers, rail joints, ballast, and sub-grade. If the railway track has different stuffiness on track and there are too high stiffness can result an increasing dynamic force on track structure which cause the deterioration and the fatigue damage on track structure. On the other hand, the large displacements are effected by the low track stiffness, and it also causes the high bending moment in the rails. Besides that, the load distribute to the track and the track interaction force will be high if there are low rack stuffiness. If the ballast, sub-ballast or subgrade is very soft the global track stiffness will be low.

According to the Winkler hypothesis the foundation modulus C is the ratio between the local compressive stress on the support σ and the local subsidence of the support w (Esveld, 2014). It can be written as:

$$\sigma = Cw \tag{2.1}$$

σ = local compressive stress on the support $[N/m^2]$
w = local subsidence of the support $[m]$
C = foundation modulus $[N/m^3]$

2.3 Factors Affecting Ballast Degradation

Ballast breakage cause by several factors, traffic loading, degree of saturation , aggregate density, frequency, number of cycles, and confining pressure. The particle

gradation size and amount of confining pressure affect the ballast degradation, (Gupta, 2009). Increasing in confining pressure for all particles increase in material breakage, they concluded that the particle size increased because the number of contact points decreased and that can lead to higher contact pressure and increased the particle breakages. (Kashani et al., 2017) also indicated that water influence track settlement and lead to trafficability problems. Their experience found that increase in the percentages of water content on laboratory test increases the rate of settlement. Various researchers indicated that the number of load cycles is the one-factor influence of the plastic deformation of ballast and other granular material such as the settlement in the samples of testing increased rapidly at the initial stage of cyclic loading. After that, the aggregate becomes stabilized, and the settlement rises slowly along with increasing number of load cycles. Then, there was an investigation on how the frequency affects the permanent deformation and degradation of railway ballast by using a series of large-scale cyclic triaxial tests. Their studies found that increasing the frequency and number of load cycle result in the permanent deformation of ballast and the particle breakage increasing (Sun et al., 2014). (Selig and Waters, 1994) conclude that ballast with low density leads to high plastic strains and higher specific gravity showed less breakdown for the ballast materials.

2.4 Laboratory Testing Methods for Studying Ballast Degradation

The significant deterioration and breakage of ballast comes from train loading. Also, the maintenance of ballast (tamping, transporting or handling) and weather condition are also factors of ballast degradation (Selig and Waters, 1994). The impact of ballast breakage causes many failures of track alignment and reduces the ability of track as mention at last sections. In addition, many researchers have proposed various methods on laboratory testing to study ballast behavior. (Koohmishi and Palassi, 2018) studied the degradation of aggregate during maintenance activities by using lab-scale compression test with the multiple steps loading and test on different material aggregate. This test uses three degradation index to quantify the amount of degradation ballast sample. The result performs that there are more degradation in ballast resulting from the maintenance of particles and lower compressive load causes less degradation. However, this test covered only compress pressure, seems to be dissimilar to rail force which lack of vibration and impact behavior.

Figure 2.7 Crushing test apparatus (Koohmishi and Palassi, 2018)

(Cuelho et al., 2008) experimented on laboratory test of Micro-Deval, LA abrasion, Sodium Sulfate, and Magnesium Sulfate to find out which method is the better quality of aggregate durability tests based on laboratory test data around the USA. They summary that the Micro-Deval is the most conservative analysis followed by Magnesium Sulfate, Los Angeles Abrasion (L.A. Abrasion) and Sodium Sulfate tests, respectively. However, there are some inconsistent testing methods because these test methods can predict the actual behaviors in the field, so to assess the important attribute, the full-scale field test have to be studied.

(Aursudkij et al., 2009) carried out the laboratory study on railway ballast under triaxial conditions and in a railway test facility which both methods determined the strain and ballast breakage. The large-scale triaxial test was designed, manufactured, and constructed to perform cyclic testing at different confining pressures, frequencies, pulse shapes, and drainage conditions while a railway test facility built in a concrete pit and comprises the sub-grade material, ballast, and three sleepers which simulated traffic loading by hydraulic actuators. The result performs that the horizontal stress and bearing stress under sleepers under a railway test facility are similar to triaxial test. The advantages of both methods simulated that the load applied to the sample was quite identical to the rail force especially the railway test facility which was identical to the real site condition and this test can measure the ballast settlement and ballast breakage by sieve analysis.

Figure 2.8 Large-Scale Cyclic Triaxial Test Equipment, Loading Machine, and Data
Acquisition System (Ebrahimi et al., 2010)

There are any numerical experimental studies that have been completed on
ballast mixed of other material under repeated loading by using ballast box test which
can apply to define ballast breakage and deformation as show on table 2.1. The box
test is a simulation segment of railway track structure and simulated ballast behavior
and ballast performance tested on field condition. Where ballast is located in a box
with a sleeper section and the cyclic loading simulated the traffic load by using
hydraulic actuator apply load through rail or sleeper section. The deformation during
loading repetitions was measured through instrumentation in each layer with linear
variable differential transducers (LVDTs).

(Selig and Waters, 1994) studied the ballast breakage by using the box test to
simulate field loading conditions which the box test apparatus for this test shown in
figure (2.9) the box was applied and repeatedly loaded by a servo-hydraulic testing
machine and the bottom of the box is flexible to denote the effect of subgrade. The
degradation was considered in two categories; the first was the coarse breakage and
second was the fine breakage. From the test that increased in wheel load from 160 kN
to 220 kN found that the fine particle increase twice the amount and the coarse
breakage increased triple of its amount. In another test, they studied the degradation
of ballast by one sample test in haft million cycles without maintenance and another
one load in haft cycles also but the ballast has to be maintenance after one hundred
cycles. They found that the ballast maintenance after each hundred cycles increased
the amount of fine more than double and amount of coarse generate triple in
compared with ballast without maintenance.
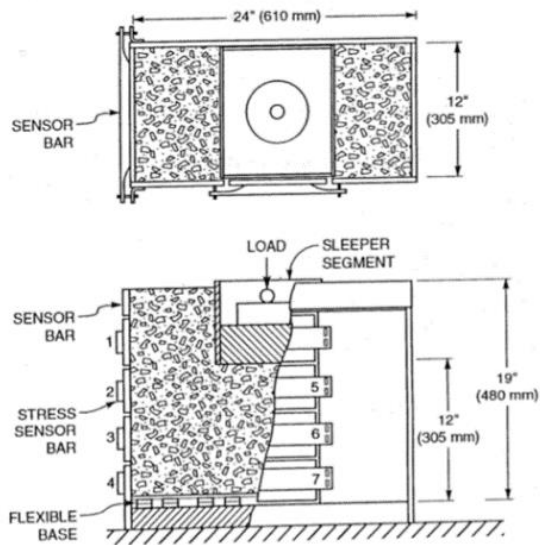
Figure 2.9 Ballast box test (Selig and Waters, 1994)
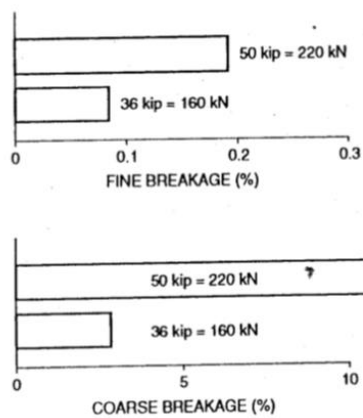
Figure 2.10 Effect of wheel load on **Figure 2.11** Effect of maintenance on
ballast breakage (Selig ballast breakage (Selig and
and Waters, 1994) Waters, 1994)
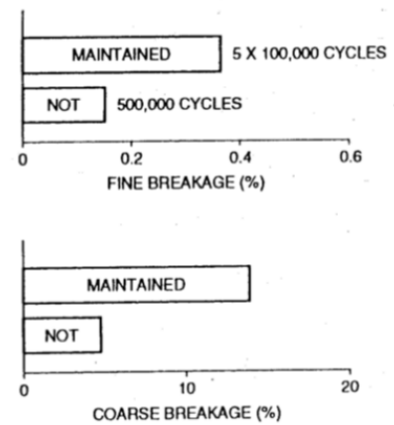
Table 2.1 Summary of the development of ballast box and the objective of research.

No	Source	Box dimention LxBxH (mm)	particle size/type of ballast	Reinceforce material	load	Objectives (study the effect of:)
1	(Raymond, 2002)	900x20x325	the ceramic Denstone	LG400, Stratagrid 200, and four bound layers Stratagrid 200	10,000 cycles at 0-40kpa	plastic settlement, aggregate breakdown
2	(Indraratna et al., 2006)	800x600x600	coarse aggregate, Dmax = 60mm	geotextile, geogrid, geocomposite.	100,000 load cycle at 15Hz	deformation and degradation
3	(Ho et al., 2013)	600x305x460	standard ballast stone	recycled tire ruber, epoxy bidder and resiliently bound ballas	100,000 load cycles at 2Hz	ballast breakage, abrasion
4	(M. Sol-Sánchez et al., 2015)	460x200x300	crashed hard stone composed of granodite, Dmanx = 50mm	Crumb rubber	100,000 load cycle at 4Hz, 200 kpa and 300 kpa stress over ballast surface	degradation, stiffness, dissipate energy and track settlement
5	(Fathali et al., 2016)	700x290x400	crashed stone of dolonite ,Dmax = 63mm	Tire-derived agrgregate (TDA)	100,000 load cycles at 3 Hz	abrasive behavior, shear strength, the particle breakage, ballast settlement
6	(Liu et al., 2016)	2440x1830x1020	Limestone, Dmax 60mm	Geogrid	500 load cycle at 1 Hz	horizontal translation and rotation, stiffness
7	(Suku et al., 2016)	900x900x600	Subgrade soil with Dmax= 60mm	Geocell	3000 loads cycle at 1 Hz.	deformation
8	(Esmaeili et al., 2017)	700x300x450	Dolomite ballast	tire derived aggregate(TDA)	100,000 loads cycle at 3 Hz.	Settlement, ballast breakage and damping ratio
9	(Du Plooy and Gräbe, 2017)	2400x600x400	-	rigid polyurethane foam (RPF)	5,000,000 load cycles at 10 Hz	ballast breakage index, ballast settlement, Resilient modulus,
10	(Kashani et al., 2017)	1320x840x520	Crushed granite stone ,Dmax=60mm	-	2,500,000 load cycles at 1 Hz	Test on water content condition , Plastic settlement

There are several quantitative methods of ballast breakage used to estimate base on the particle size distribution before and after test discussed below.

(Marsal, 1967) put forward an index of particle breakage $\left(B_g\right)$ by utilizing the initial and final particle size distribution (PSD) curve, determined the variance in percentage retained on each size$(\Delta W_k = W_{ki} - W_{kf})$, where W_{ki} is the percentage retained on the sieve size k before a test and W_{kf} is the percentage retained on the sieve size k after a test. Marsal defined the ballast breakage $\left(B_g\right)$ expressed as a percentage by sum of the positiveΔW_k.

(Lee and Farhoomand, 1967) put forward breakage indicator to express the amount of particle breakage by using ratio for the initial size of 15% for the particle $(D_{15})_i$to a size of 15% after testing$(D_{15})_f$.

$$B_g = \frac{D_{15i}}{D_{15f}} \tag{2.1}$$

(Lade et al., 1996) introduced particle the breakage factor base on D_{10} which has the size between 0.1 and 3 mm. The particle breakage factor can be calculated from the equation (2) where D_{10f} is the effective grain size of the final gradation, and D_{10i} is the effective grain size of the initial gradation.

$$B_{10} = 1 - \frac{D_{10f}}{D_{10i}} \tag{2.2}$$

(Indraratna et al., 2005) suggested a new Ballast Breakage Index (BBI) to determine the breakage of railway ballast specifically. The calculation of BBI based on a change of the Particle Size Distribution (PSD) of the ballast before and after testing. The BBI can be calculated from equation (3), where the parameter A is the area enclosed by ballast particle size distribution diagrams before and after testing. B is the area bounded with final ballast gradation and the arbitrary line of maximum breakage.

$$BBI = \frac{A}{A + B} \tag{2.3}$$
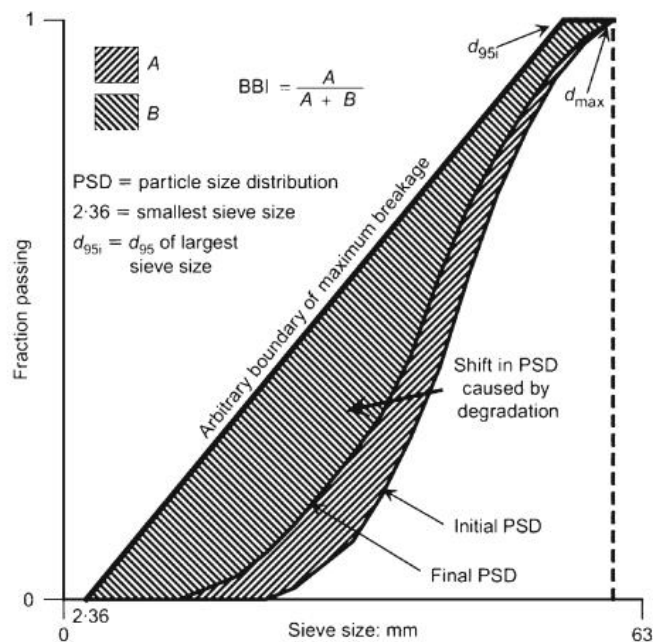
Figure 2.12 Ballast breakage index (Indraratna et al., 2005)

The method expressed above, mostly used the sieving material before and after the test. Throughout the last period, apparatus vision technology and image segmentation have been applied as an objective and accurate tool for measuring size of particles and figure properties in a rapid, reliable and automated fashion when the manual methods was compared (Qian et al., 2015). There are laboratory and field studies on assessing ballast degradation properties using Los Angeles Abrasion (LAA) testing and imaging techniques. The technique of using Enhanced-University of Illinois Aggregate Image Analyzer (E-UIAIA) shows the successful result to detect the change in shape and size of the particle (Qian et al., 2014).

(Vadood et al., 2014) determined size of aggregate in hot mix asphalt using image processing. The process of this studies has to cut the cylindrical sample into five thin slices and use the photos from the cutting surface to separate rock out of bitumen by the binary image. The researcher chose the color space method in separating image and then used distance and watershed transform to find the edge of aggregate. The area, minor and major axis are defining from the vellum of the pixel which fit with the diagonal. The result from image processing found that it capable of estimate the aggregate size (maximum aggregate size 12.5mm and 19mm).

2.5. Reducing Ballast Degradation
2.5.1 Alternatives

As described from the last sections the ballast degradation can cause many failures on the railway track, and the result to ballast breakage is the regular method maintenance tamping which has unfavorable effect until the replacement of ballast to

improve track alignment and the ability of load-bearing capacity. To avoid the more frequency of ballast layer maintenance, more granular stabilization techniques were studied to improve the mechanical properties of ballast aggregates such as: the using of two-dimensional reinforcements [geogrid, geotextile, geocomposite (combination of geogrid and geotextile)] capable of reducing the track disability as confirmed through the laboratory test setup (Indraratna et al., 2006). Since the last period, these were the studies of ballast improvement by elastic material which has numerous benefits such as improve the track stability alignment by reducing ballast breakage as well as reduced noise and vibration, thus improving the of the track structure as discussed below.

2.5.1.1 Under Sleeper Pads

Under sleeper pads (USP) are resilient element attached under sleepers as an attachment to provide additional track resiliency between the sleepers and ballast. The common aims for using USP are to moderate track stiffness; to reduce ground vibrations, and to reduce ballast breakage. There are studies about under sleeper pads (USP) with a thickness of 10mm placed under the concrete sleepers to improve rail track resilience. In order to protect ballast (Hunt and WINKLER, 1997; Lundqvist and Dahlberg, 2005) had recommended that the use of under sleeper capable of reducing stresses between ballast and sleeper contract was the better solution used to increase life cycle of ballast track. From the field trial over a year, found that USP attached under sleeper tend to reduce the sign of ballast breakage under and surrounding USP sleepers. Moreover, there is the usage of recycle vehicle tires as elastic elements in railway by studying the influence of thickness, the resistance capacity of the element and their behavior in a ballast box (Kaewunruen and Remennikov, 2015). According to their experiences found that the USP from used tires (thickness between 4-11.5mm) is appropriate stiffness value to be used as soft elastic elements in railway track even though this rubber is thinner than standard USP which has the thickness up to 20mm (M. Sol-Sánchez et al., 2015).

Figure 2.13 Under sleeper pads (Kaewunruen and Remennikov, 2015)

2.5.1.2 Crumbed Rubber Particles

Crumb rubber is the material derived from scrap tires or other rubber into uniform granules. In order to reuse this material, there was the use of crumb rubber to increase the service life of track by mixing these elastic materials into ballast particles, they found that it capable of minimize ballast cracking and renewable of mountain aggregates. The samples were in any box test compose of different ratios of tire rubber. The study focusses on measuring ballast deformation and stiffness of ballast particle in box. The breakage of particles is quantified in each test which has to measure before and after the test. The result shows that crumb rubber of 10% by volume of could reduce ballast breakage and its stiffness is reduced. The used of elastic aggregates with 10% also could reduce the track settlement base on the laboratory study (M. Sol-Sánchez et al., 2015).

Moreover, (Fathali et al., 2016) evaluated the performance of ballast materials influenced by the tire-derived aggregate (TDA) . The test used the waste TDA mixed with ballast in the same gradation to reduce ballast degradation and deformation. The ballast box with the dimension of 700 mm long, 290 mm wide, and 400 mm high was used to prove the deformation ballast behavior, and the ballast breakage under cyclic sinusoidal loads at a frequency of 3 Hz and applied maximum number of load cycle to 100,000 cycles on box (285 mm in width, 215 mm in length, and 100 mm in height). The tests on ballast samples studied on pure ballast, 10% and 20% by weight of TDA. The result showed that the degradation of ballast without elastic material would be reduced up to 47.48% and 70.50% for 10% and 20% TDA.

Figure 2.14 The ballast and crumb rubber material mixing in box apparatus
(M. Sol-Sánchez et al., 2015).

2.5.1.3 Ballast Mat

In order to reduce the vibrations and energy absorption from wheel load of train, there were the used of an elastic anti vibration mat in which place under the

ballast layer. This elastic material is essential using in rigid foundation where it used to reduce stress on the substructure as well as vibrations and noise levels. Even these elastic elements are vary in design and composition, all of these elements are able to reduce the impact of wheel loads and the vibrations when the train run through (Miguel Sol-Sánchez et al., 2015). The track performance also can maintain even it had load repeatedly with high number cycles and in varied weather condition. Moreover, there were uses of recycled automobile tires as the ballast mat and laboratory test found that it caused an increase in the ballast deformation as a result of affect to low stiffness and increase of dynamic movement which could be suitable to minimize track deterioration (Sol-Sánchez et al., 2014).

2.5.2 Influences on railway track
2.5.2.1 Track modulus

The track modulus is affected to the components of railway track in clouding ballast layer. The study of elastic material to improve the ballast layer in order to reduce ballast breakage and settlement shows that the uses of rubber material not only effected on ballast but it also changes the track modulus on this structure. According to the laboratory test on using crumb rubber, they found that use of high amounts of rubber particle (twenty percent and thirty percent by volume) capable of producing an excessive vertical deflection and increasing in track stability which mean that the stiffness of ballast is also decrease. The decreasing of ballast stiffness is the same as the decreasing of track modulus which effect the high settlement of ballast layer that also effects to another track component to become deterioration and need more track maintenance cost (Sol-Sánchez et al., 2014).

2.5.2.2 Life Cycle Cost

The ballast by weight and by volume is the main factor of the track, and it is a important part of the entire civil engineering budget of the railways on buying and distributing ballast on construction and maintenance. In order to reduce the number of works needed to maintain existing ballast track, researches and developments of methods was conducted to minimize the track maintenance that effect on train operations such as TC Type Low-Maintenance Track which have superior labor-reduction characteristics and cost-effectiveness. Furthermore, the adding crumb rubber makes the settlement rate lower by comparing with the reference sample, which shows that using of ten percent of small tire rubber had good result and if this behavior happed during the hole service life of the material it could improve the long-term the ballast layer behavior**.** It can be summarized that the use of small piece of tire rubber used as particle mixture in ballast layer is appropriate to reduce the track deterioration associated with the ballast deformation and reduce maintenance work which is budget consuming (M. Sol-Sánchez et al., 2015). In the same way, the use

of geocomposites in recycling ballast to reduce the breakage index was used, and the use of geosynthetics can stabilize the recycle ballast which would be cost-effective option to minimize the cost of track maintenance (Indraratna et al., 2006).

CHAPTER 3
METHODOLOGY

3.1. Overview of methods used in this research

This research focus to study the use of Para rubber for reducing ballast deterioration, the testing plan consists of the study of Para rubber in a ballast box which has the dimension of 60cm long, 35cm wide, and 45cm high which the similarly to the box by (Selig and Waters, 1994) that can use in measuring and observing ballast degradation. This ballast box simulates the railway track bridge or tunnel which is the ballast layer place under the rigid sub-ballast.

In order to analyze the influence of alternative methods in applying Para rubber to improve ballast performance. Three alternatives ware prepared as follows.

1) Para rubber Ribbed Smoked Sheets were cut in the sheet with the thickness of 15mm and attached beneath the sleeper in order to act as an under sleeper pad.
2) Para rubber Ribbed Smoke Sheet were cut in the sheet with the thickness of 15mm and attached at the bottom of the box to act as a ballast mat.
3) In addition, the pure ballast without any natural elastic particles were also analyzed to use as a reference case study.
4) Besides that, an under sleeper pad is placed under the bottom of sleeper which is a commercial material also use as one reference in this study.
5) In the same way, a commercial ballast mat was fasten under the bottom of the box. This case was tested as a reference because it is a widely used elastic solution.

The box was placed in the load frame to provide vertical repeated loading from the hydraulic testing machine, and the amount of load applied to sleeper segment was determined from GEOTRACK analysis which relates to the ballast pressure at the bottom of the sleeper. The number of loads consisted of one million cyclic sinewave loads at 5Hz frequency. The number of the cyclic loads equal twenty million tons of axle load passage of Thailand railway.

3.2. Box Test to Evaluate the Effects of Alternatives on Ballast Degradation

Before taking the ballast into the box, it had to be cleaned by water to remove out of dust or dirt in aggregate texture. Then dried the aggregate until all water has left the sample by the oven at the temperature of 105-110 degree Celsius for overnight according to AASHTO T 85 standard. According to this research aim, the ballast breakage was studied by using image processing. So, ballast aggregate was taken a photo to find the initial particle sizes information by image processing. Before taking the picture of aggregate, the texture of each aggregate had to mark the sign in each zone as show in **Figure 3.1** to study which zone is the most affected and observe the degradation of each zone.

Crib	Sleeper Segment	Crib
L2-	M2-	R2-
L1-	M1-	R1-

Figure 3.1 Box sampling zone and sign.

Figure 3.2 Visualizing appearance and placing of the ballast in the box.

After marked and took photos of ballast, the ballast aggregate was poured into the box and separate the zone of ballast by steel place. The ballast in this study had two layers, each layer had the thickness of 150mm and compacted by a vibratory hammer. Then a plate rectangular concrete (250mm x 300 mm x 150 mm) simulated a portion of the sleeper was placed on the center of the ballast layer. The space between the sleeper and vertical walls was filled with crib ballast with the 150 mm thickness. After the sample preparation finish, it had to move to the Servopulser machine in order to apply the cyclic load.

The cyclic vertical load was applied to sleeper by a dynamic actuator. The ballast was repeatedly loaded with a sine wave load pulse at the minimum load of 0.4kN and maximum load of 28KN (roughly equivalent to a passage of an axle load of 20 tons). In this testing, the 0.4kN is the seating load which is a load of sleeper and rail. While the axle load of 20 tons becomes to a load of 28kN used to apply to the sleeper was calculated from the Geotrack program and the dynamic load factor. In this calculation, it was separated into two section which the first the is to find the pressure under the sleeper and the second section is to find the maximum dynamic load factor. According to the calculation **(a), (b),** and **(c)** could found that axle load of 20 tons can be scale to use in this testing with the maximum of 28kN apply to the concrete section of 25x30cm.

During the repeated load test, all peak loads and peak deformation measurements are continuously recorded.

At the end of each test, the ballast is taken out of the box systematically to identify the change in grading by using image processing method and the changing of particles by scaling in each particle.

3.2.1 Ballast pressure.

In order to simulate the load of train pass through the ballast track, the pressure under the sleeper is estimated base on two methods as follows:

3.2.1.1 Methoth#1 AREMA Manual's Ballast –sleeper pressure.

The American Railway Engineering and Maintenance-of-Way Association (AREMA) Manual for Railway Engineering presents an estimating of sleeper-to-ballast pressures by **Equation 3.1** which is the simplified uniform load**.** In this calculation, the AREMA recommends that the average pressure at the bottom of the sleeper should be calculated as the axle load multiplied by distribution and impact factors and divided by the bearing area of sleeper as show in Equation 3.1 (AREMA, 2011)

$$P_{avg} = \frac{(2P) \times \left[1 + \frac{IF}{100}\right] \times \left(\frac{DF}{100}\right)}{A} \tag{3.1}$$

Where P_{avg} is the average bearing pressure at the ballast-sleeper interface.

P is the applied wheel load.

DF is the distribution factor which estimated by the **Figure 3.3.**

IF is the impact factor.

A is the bearing area of the sleeper.
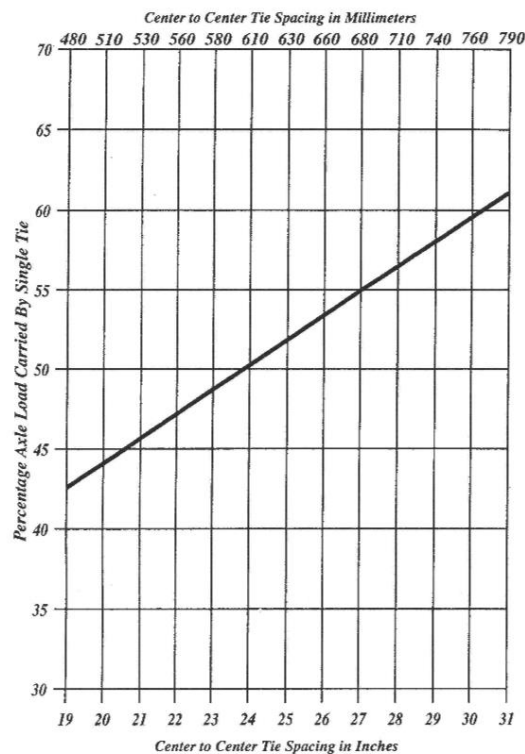
Figure 3.3 Percentage of axle load carried by a single conventional sleeper for varying spacing – the distribution factor (AREMA, 2011)

According to the Figure 3.3, the spacing of SRT sleepers is 60 cm. so that the distribution factor is 50%. The bearing area of the sleeper using in State Railway of Thailand is 252mm wide and 2000mm long. While the impact factor used in the study cover with two conditions as below:

A. Condition no impact factor.

$$P_{avg} = \frac{(2P) \times \left[1 + \frac{IF}{100}\right] \times \left(\frac{DF}{100}\right)}{A}$$

$$P_{avg} = \frac{(2 \times 98066.5) \times \left[1 + \frac{0}{100}\right] \times \left(\frac{50}{100}\right)}{252 \times 2000} = 194 \, Kpa$$

Load happen under sleeper = 194 x 2 x 0.252 = 97.776 kN.

B. Condition impact factor equal to 200% according to assumption of AREMA

$$P_{avg} = \frac{(2P) \times \left[1 + \frac{IF}{100}\right] \times \left(\frac{DF}{100}\right)}{A}$$

$$P_{avg} = \frac{(2 \times 98066.5) \times \left[1 + \frac{200}{100}\right] \times \left(\frac{50}{100}\right)}{252 \times 2000} = 583 \ Kpa$$

3.2.1.2 Method#2 GEOTRACK Analysis.

GEOTRACK is the software that is used to analyze the track structure under vertical dynamic loads (Selig and Waters, 1994). GEOTRACK is a three-dimensional , multi-layer elastic model which estimated the track structure base on the material parameters, track geometries, load, and properties of ballast in the program and then the results of the analysis are stresses shown on **Figure 3.4**.
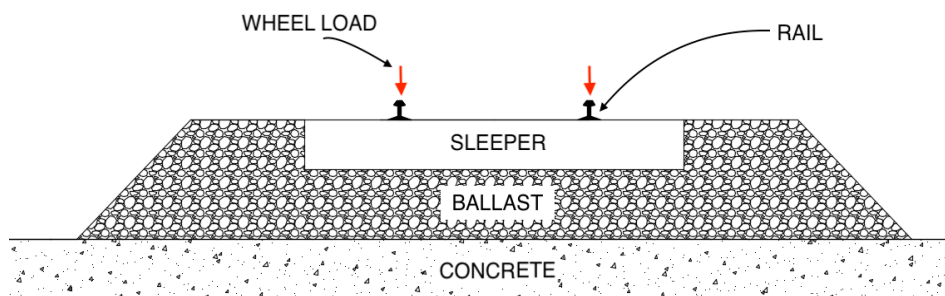
Figure 3.4 Typical cross section of a ballasted track

Figure 3.4 shows the cross section of ballast place on the rigid foundation. The properties of material and track geometries used in GEOTRACK are given below:

- Rail properties
  E = 200 GPa
  I = 1.961 x 10^{-5} m^4
  A = 6393 mm^2
  Gauge = 1.000 m
  Rail weight (kg/m) = 50.18
  Rail Fastener stiffness (kN/mm) = 7.981 x 10^5
- Sleeper properties
  Load applied at 1st sleeper
  Sleeper spacing = 60 cm
  Sleeper length = 2000 mm
  Young's modulus of sleeper = 3x 10^4 MPa
  Sleeper weight = 264 kg
  I = 2.42 x 10^8
- Substructure properties
  Resilient modulus of ballast = 350 MPa
  Thickness of ballast = 300 mm

Resilient modulus of subballast = 200 MPa

Thickness of subballast = 300 mm

Subgrade assume as concrete Mr = 30,000 MPa

- Load

  Wheel load = 10 tons
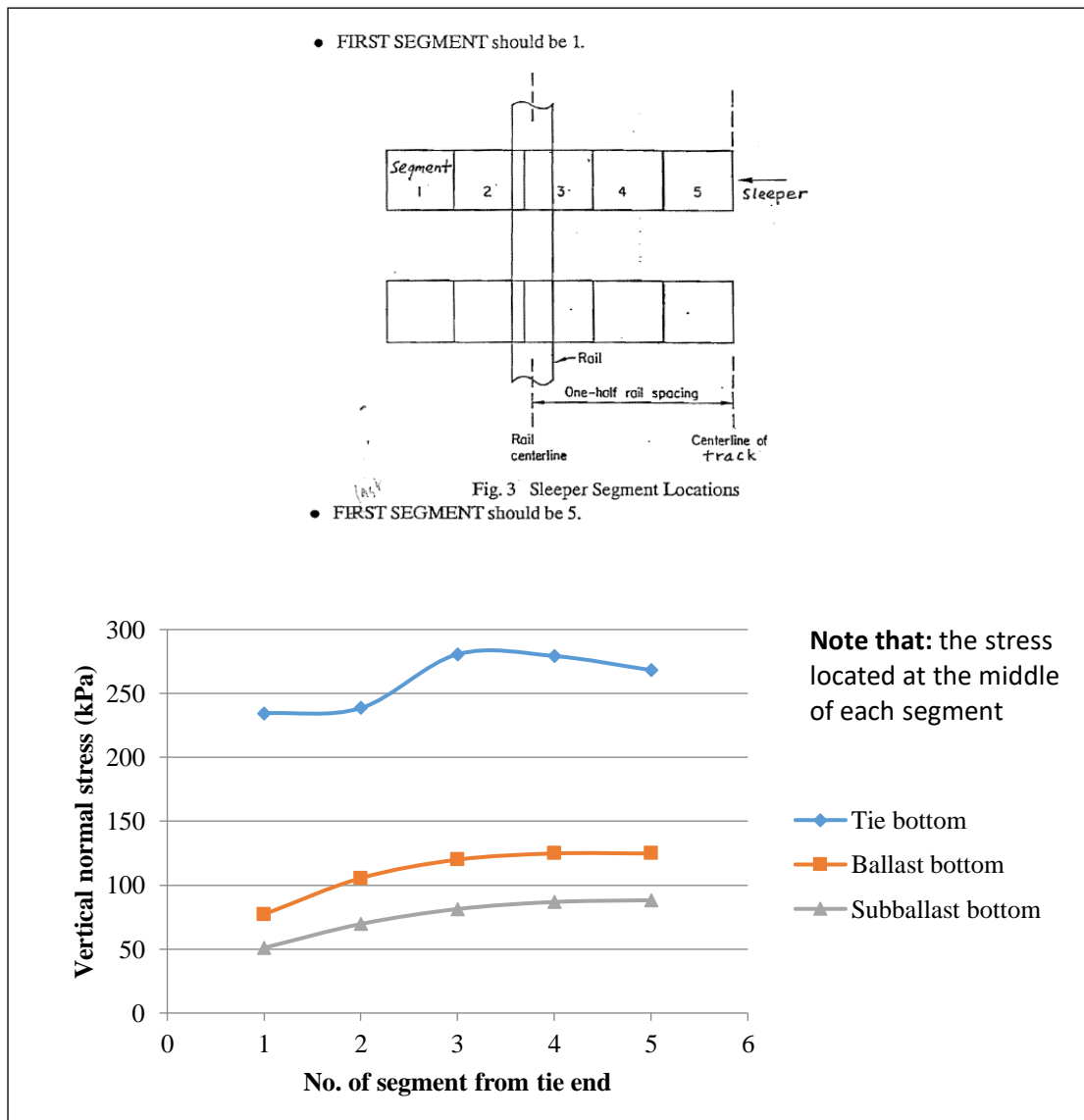
Figure 3.5 Stress estimation on segments of sleeper by GEOTRACK analysis.

From the result of GEOTRACK analysis in the **Figure 3.4** found that the highest stress was at 280.69 KPa and the lowest was at 234.48 KPa. The average stress happened on the entire of sleeper in this model was around 260.27 KPa. In order to define the force underneath the ballast and sleeper, the vertical stress from GEOTRACK was multiplied by area in each section of sleeper and sum all of load. The dimension of sleeper using in State Railway of Thailand is 252mm wide and

2000mm long. The GEOTRACK analyst the half sleeper so that the load under half sleeper was calculated as following:

$$F_n = \sigma_n \times A_n \quad \text{n is number of sleeper segment} \tag{3.2}$$

$$F_1 = \sigma_1 \times A_1 = 234.48 \times (252 \times 200 \times 10^{-6}) = 11.817 \; kN$$

$$F_2 = \sigma_2 \times A_2 = 238.65 \times (252 \times 200 \times 10^{-6}) = 12.027 \; kN$$

$$F_3 = \sigma_3 \times A_3 = 280.69 \times (252 \times 200 \times 10^{-6}) = 14.088 \; kN$$

$$F_4 = \sigma_4 \times A_4 = 278.31 \times (252 \times 200 \times 10^{-6}) = 13.971 \; kN$$

$$F_5 = \sigma_5 \times A_5 = 268.28 \times (252 \times 200 \times 10^{-6}) = 13.521 \; kN$$

$$F_1 + F_2 + F_3 + F_4 + F_5 = 65.424 \; kN$$

3.2.1.3 Maximum dynamic wheel load

The stress under sleeper from both methods are relate to the data measured on the real railway track structure but in the construction design of railway need the maximum value so that it has to be added others factor in order to increase its value as **Equation 3.2** (Vanicek and Vanicek, 2008).

$$\max Q = Q_{mean} \times (1 + t.n.\varphi) \tag{3.3}$$

where

t is the reliability factor

n is track condition factor

φ is speed factor

- For the reliability factor

Table 3.1 The reliability factor

Reliability level (%)	68.3	90	95	99.7
t	1	1.65	1.96	3

- For the track condition factor

Table 3.2 Track condition factor

Track condition	Example of route (In Germany)	n
Very good	Main intercity route	0.1
Good	Secondary intercity route and suburban train	0.15
Bad	Another route	0.2
Very poor	-	0.25

- For the speed factor, φ can get from:

  If speed $V < 60\frac{Km}{h} \rightarrow \varphi = 1$

  If speed $V \geq 60\ Km/h$ there are two conditions:

  For passenger train $\varphi = 1 + \frac{V-60}{380}$

  For freight train $\varphi = 1 + \frac{V-60}{160}$

3.2.1.4 Summary of applied load determination

In both method AREMA and GEOTRACK found that they differ around 24.12% in comparison based on no impact factor condition. The AREMA method is the simplified uniform load while GEOTRACK is three-dimension model. Therefore, in this study the result from GEOTRACK analysis was used because this method is the development of advanced computational tool and the result base on parameters in the railway structure.

From **Figure 3.5** the result of GEOTRACK analysis, found that the axle load of 20 tons causes the maximum pressure under sleeper equal to 280.69 KPa. In this study use the maximum pressure because this value capable of cover all stress under sleeper than average value. In term of the reliability on this test used the reliability level of 99.7% because we need the high reliability on the test so that the reliability factor used in this study was $t = 3$, also as the track condition we assume that our track structure in main intercity route which is very good track condition so the track condition factor was $n = 0.1$, and the speed of freight train equal to 80 Km/hr in which the speed factor will equal to 1.125. Our sleeper was the size of 25x30 cm so that the load for testing can be calculated as follow.

$$\max Q = \ 280.68 \times (0.25 \times 0.3) \times (1 + 3 \times 0.1 \times 1.125) = 28.15\ kN$$

3.3. Used Materials and Its Properties

The ballast used in this study is originated in Saraburi province. It is composed of Dyorite stone used for railway track ballast in double track construction project in 2018. The main physical and mechanical properties of aggregate tested gradation, bulk specific gravity, LA abrasion, and soundness to indicate that the ballast material is appropriate to be used as ballast in railway tracks according to SRT specification.

Figure 3.6 Visual appearance of ballast.

One thousand kilograms of ballast was obtained from the SRT construction site so we assumed that the ballast had conformed to the specification of the Redline construction below:

Los Angeles Abrasion must not exceed 25%. The percentage of wear determined in accordance with ASTMC535-Gtading 1. According to the Los Angeles Abrasion test found that the percent wear equal to 16.8% means that the ballast passes the standard specification.

Limit of flakiness index must not exceed 30% by mass. The flaky ballast is classified when the thickness is less than 0.6 of the nominal size. The flakiness index was determined in the accordance with BS812 PART 1:(1975). From the test found that the percent of flakiness index was equal to 12.7%. So, the ballast particles had an excellent condition and passed the standard specification.

The elongation index is the elongated of ballast that the length (greatest dimension) exceeds 1.8 time the nominal size and the elongation index must not exceed 30% by mass. The elongation was determined in accordance with BS812 PART 1:1975). According to the result of testing found that the elongation index equal to 9.7% means that the property of ballast passed the standard specification.

Figure 3.7 shows the ballast grading used in this study together with the SRT specification for comparison.
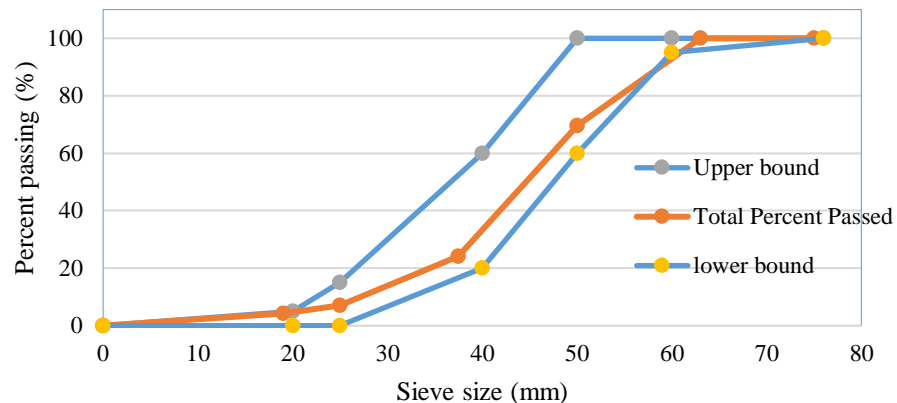
Figure 3.7 Gradation of ballast used in this study.

The Para rubber used in this study was processed in a form of rolled and smoked sheet which was produced from agriculturist. The originating of this Para rubber was from Nakhon-Si-Thammarat. The reason to use this Para rubber for testing because it is a product produced from the local plantation in Thailand. The thickness of para rubber used in this study is 15mm. The visual of para rubber is shown in **Figure 3.8.**

A piece of ballast mat which is a commercial synthetic material used on the test to compare the mechanical performance with natural rubber. This rubber mat was cut to size to place on the bottom of the box to simplify a common elastic solution that employed under the ballast layer in sections over rigid substructure. The thickness of the ballast mat in this study is 15 mm. Moreover, the commercial ballast mat was also used as under sleeper pad. The physical properties and material composition of commercial ballast mat are shown in **Figure 3.9** which are found that elastic modulus of para rubber equal to 4.01 MPa and the elastic modulus of commercial synthetic sheet equal to 3.16 MPa. The elastic modulus was defined by the stress per recovering strain of the material. Both values of elastic modulus were chosen from the average of elastic modulus in each cycle when the stresses of both were stable.
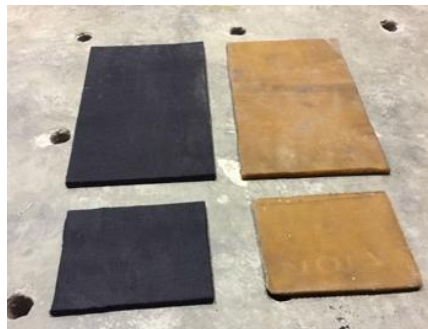
Figure 3.8 Visual of commercial material and para rubber use as ballast mat and USP.
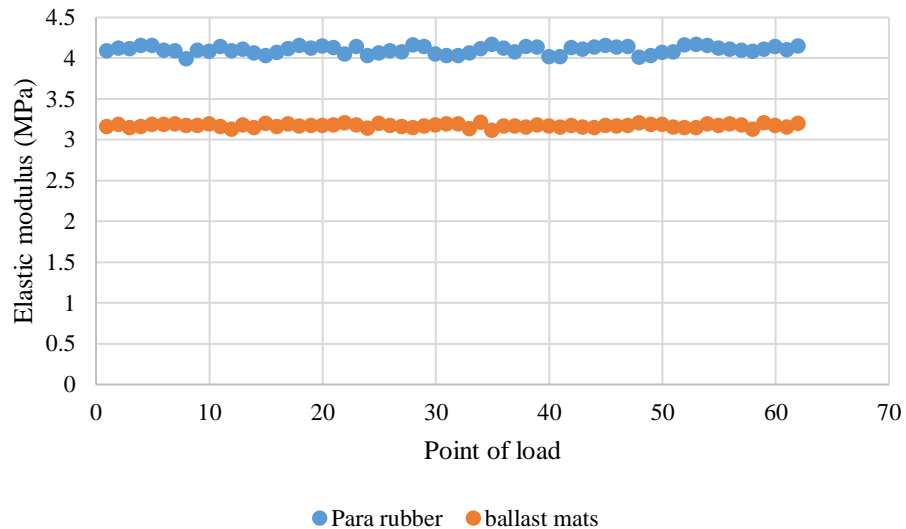
Figure 3.9 Elastic modulus of para rubber and commercial material.

3.4 Testing tool

In this research, the test was separated into two parts, image processing test and cyclic test, which used different tools as described below:

3.4.1 Image analysis tools

1) The tool used to weigh the particle is the electronic scale that can be read to 0.01g as shown in **Figure 3.11**.

2) For photography tools, there is a camera, a tripod, Acrylic sheet, white papers, and the lights. Taking the photo in this study shown in **Figure 3.10**, the object was place on the acrylic sheet and the light placed under ballast to make the particle has black color, and its edge be the same color. Then the camera was shooting on the top view. For side view also use the same method to change the position of material and line the particles in one line. This method is used to separate the particle out of background because some particle its edge has the same color of background when analyzing the image its edge will be the loss.

Figure 3.10 Camera and imaging equipment

Figure 3.11 Scale for weighting the ballast.

3.4.2 Cyclic test tools

The cyclic tests were performed using a SERVOPULSER hydraulic test machine. The test arrangement is shown in **Figure 3.12** and **Figure 3.13** which cover of steel ballast box, Servo-pulser hydraulic machine. All ballast particles were marked the numbers of each zone. Then they were placed in their designated zones in the ballast box and compacted using a vibratory hammer. Then the sleeper and cribbed ballast were placed on top of ballast. The full box was moved into the loading frame (**Figure 3.13**. c) which loaded the pressure to the sleeper in order to simulate the trainload. The load pattern and a number of load cycle were controlled through the controller (**Figure 3.13**, b) and it is also the machine used to collect data.

Figure 3.12 General view of ballast box apparatus

a. Testing machine

b. Controller   c. Loading frame
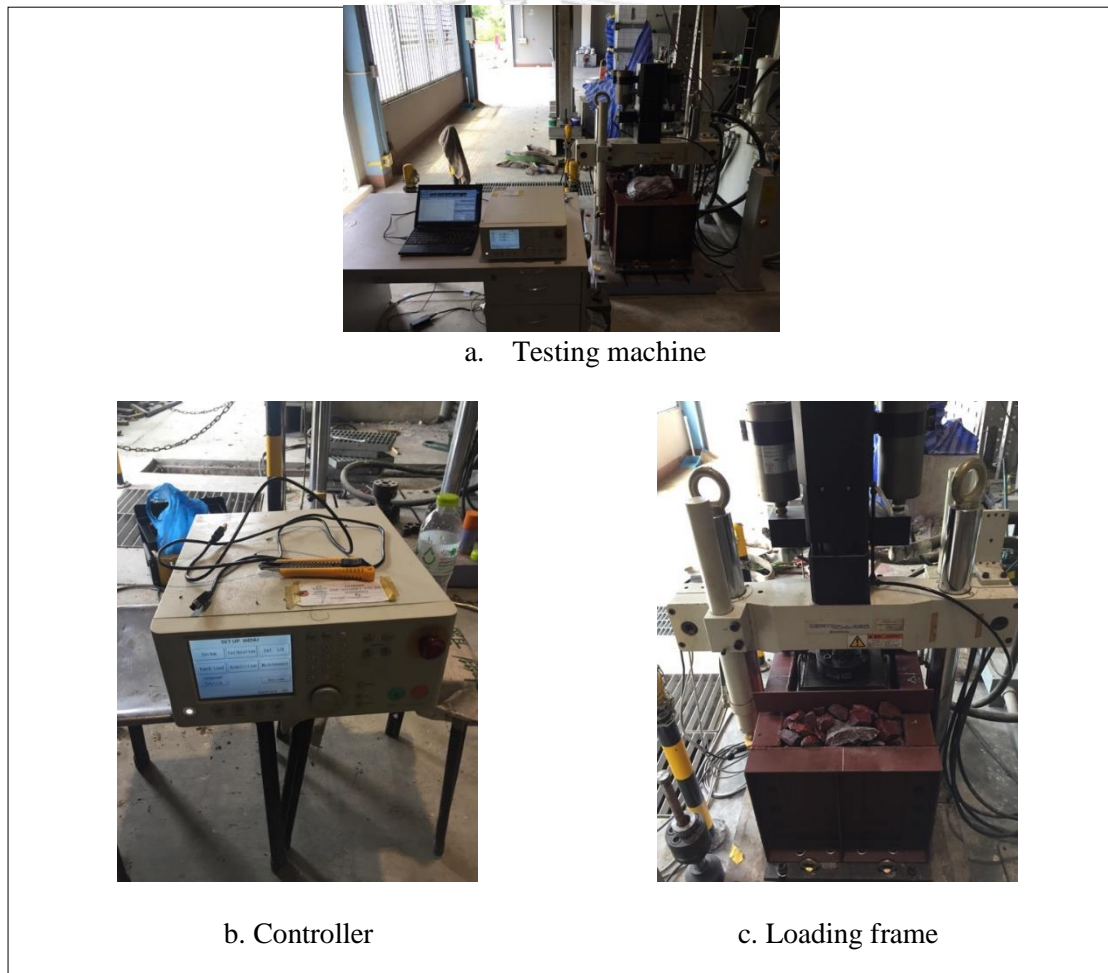
Figure 3.13 SERVOPULSER system and process simulation

The simulated cyclic loading of passing train was achieved by applying sine-wave loading between 0.4kN and 28kN as shown in **Figure 3.14**. The loading

frequency used for each actuator was 5Hz, which equal to a train with a speed of 36 Km/hr. This speed is relatively lower the actual speed of freight train in Thailand however this frequency was constrained by pressure and according to (Shenton, 1978) suggest that the load frequency does not significantly affect to the deformation of ballast behavior. While testing the controller will collect the data from the machine that the researcher had set. Because the data will be huge to collect all cycle of the load so that there was a setting of collecting data in the range as shown in **Table 3.3.**
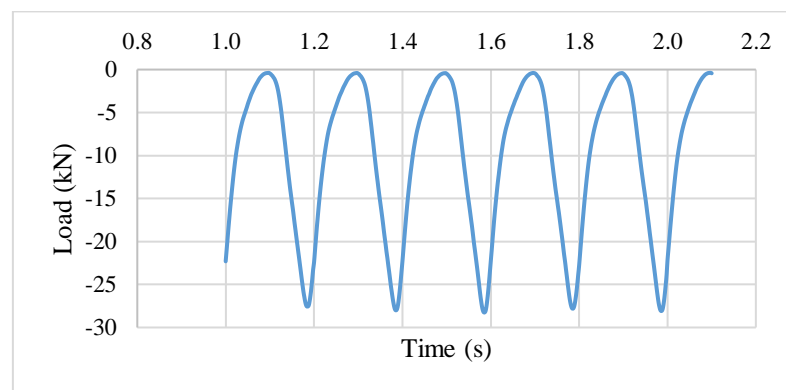
Figure 3.14 The characteristic of load pattern for ballast box test.

Table 3.3 cycles of data collecting

Stages	Cycle	Collect data	Data
Pre-condition	1-2000 cycles	Collect every 100 cycles	Load Settlement
	2000-10000 cycles	Collect every 500 cycle	
Running condition	1-2,000 cycles	Collect very 100 cycles	Load Settlement
	2,000-100,000 cycles	Collect every 500 cycles	
	100,000-500,000 cycles	Collect every 1,000 cycles	
	500,000-1,000,000 cycles	Collect every 2,000	

3.5. Experimental design cases of study

Table 3.4 summary of the test patterns and number of samples used in the test.

Study	Material and elastic element testing	Parameter study	Number of box test	testing time (day)	Tests
Ballast box study	Ballast ref (Ballast alone as reference)	Ballast deterioration	1	4	Repeated loading test (1,000,000 load cycles at 5Hz)
	Para mat (Ballast with a ballast mat using para rubber)		1	4	
	Com. Mat (Ballast with a ballast mat using commercial product)		1	4	
	Para USP (Ballast with an under sleeper pad using para rubber)		1	4	
	Com. USP (Ballast with an under sleeper pad using commercial product)		1	4	
Total testing time				20	
Image Processing				14	
Total procedure time				24	

3.6 Test Procedure and Output

Figure 3.15 shows the procedure of this study. Before testing the particles were taken photos to find the particle dimension and weighed the particles' mass by scale. After that it was added into the box and compact with a vibratory hammer in each layer. The sleeper was placed on the ballast layer with the crib beside and then bring to loading frame to transfer the cyclic load. After the cyclic test run to 1,000,000 cycles, the particle was taken off the box to separate breakage particle and foul from loading. The particles from cyclic test were also retaken photos and weighed to collect the changing of material. The Output of image processing was the dimension of the material cover of the major axis and minor axis. For the cyclic test, the output collected from the controller was load, deformation, and number of load cycle.
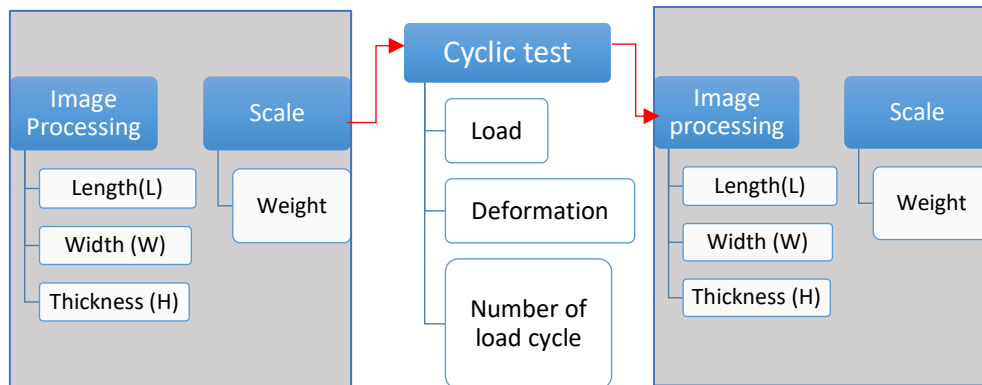
Figure 3.15 Testing process

3.6.1 Image processing

Determine the dimension of ballast by image J as follows:

1) Bring the image from the photography through the image processing using the image J program.
2) Resize an image with the program to make it in millimeter.
3) Separate the ballast and find the boundary of ballast by using Binary command from the program.
4) Calculate the area, major axis and minor axis of ballast which measure the number of pixel of each ballast using the program, and the dimension of ballast was used the ferret dimension method. The ferret diameter method is shown in **Figure 3.16.**

Figure 3.16 Analyzing image process
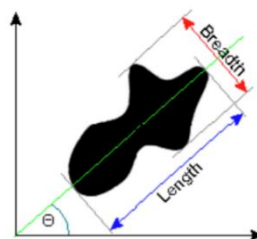
Figure 3.17 A measure of an object size by Feret diameter.

3.7 Result Analysis Method

Take the test result from the ballast box test process and image processing that perform a test base on the variables of interest to analyze the difference in each factor of the test. As shown in **Figure 3.18** shows the analyzing of output from each testing in this study. Then find the conclusion of each sample which factors influence the engineering properties of ballast degradation and how is the degradation of each sample changed.
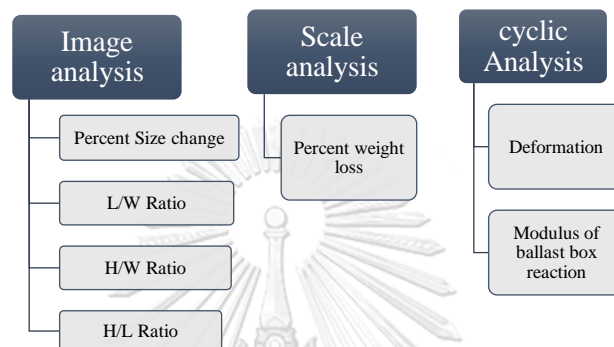
Figure 3.18 Analysis of output from testing

3.7.1 Interested variable
3.7.1.1 Independent variable

1) There are five different samples as show in Table 3.6
2) Image of aggregate

3.7.1.2 Dependent variable

1) Ballast Breakage
2) Deformation: recoverable deformation and permanent deformation

3.7.1.3 Controlled variable

1) Initial gradation of each sample.
2) Load applied to the sample.
3) Thickness of under sleeper pads and ballast mats made by Para rubber equal 15mm

3.7.2 Gradation analysis

- Take photos of ballast through the image processing process to separate the ballast out of the background by change the ballast aggregate in to white color and background into black color.

- Next take pictures that divided into black and white color to find area, major and minor axis of each aggregate by using image J.
- Then the equation below used to calculate the retaining percentage.
- Finally, plot graph of that retaining percentage.

$$S_i = \frac{A_i}{T_A} \times 100 \, ; \quad i = 1, 2, 3, \dots, n \tag{3.4}$$

- S_i is a percentage of retention of the sieve i
- A_i is the sum of aggregate area that the minor axis of ellipses smaller or equal to the diagonal of sieve i.
- T_A is sum of all aggregate area.
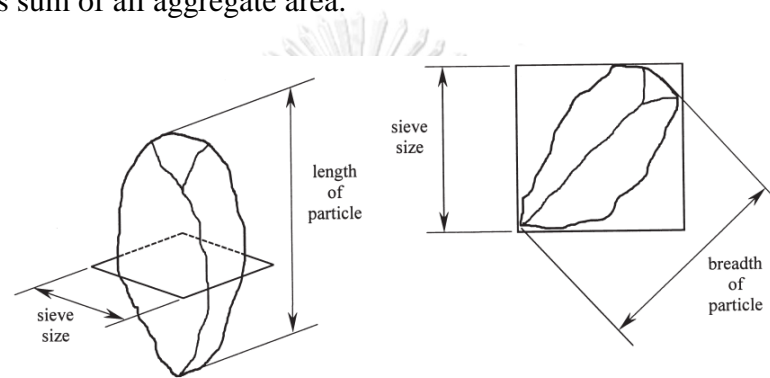
Figure 3.19 Example of thickness and breadth of particle (Kwan et al., 1999)

CHAPTER 4
RESULTS AND DISCUSSION

4.1 Ballast Degradation

After the simulation tests with one million load cycles, analysis on ballast degradation of the five box tests are conducted and presented in this chapter.

4.1.1 Fine breakage and coarse breakage

In this study ballast degradation is considered/classified into two categories namely, coarse breakage and fine breakage. Coarse breakage refers to ballast particles that are broken into pieces with size greater than 9.5 mm (3/8in.). While fine breakage describes ballast particles broken into sizes less than 9.5mm size (3/8in). Both are presented in percentage of ballast particle weight. The percentage of coarse breakage and fine breakage was calculated by the equation (4.1) and (4.2) below.

$$\text{Percent fine breakage} = \frac{W_f}{W_{all}} \times 100 \quad (\%) \tag{4.1}$$

$$\text{Percent Course breakage} = \frac{W_c}{W_{all}} \times 100 \quad (\%) \tag{4.2}$$

Where:

W_f is weight loss of particle less than sieve 9.5mm (3/8" sieve size) after test.

W_c is weight loss of particle bigger than sieve 9.5mm (3/8" sieve size) after test.

W_{all} is total weight of ballast before test.
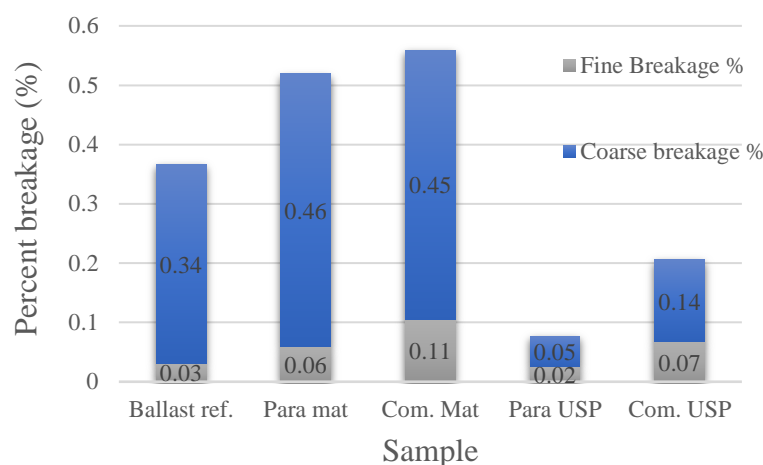
Figure 4.1 Ballast degradation.

Table 4.1 Number of ballast particles experiencing deterioration in each box case

Box case	Fine breakage particles	Coarse breakage particles	Total particles
Ballast ref	758	12	770
Para mat	801	25	826
Com mat	759	26	785
Para USP	797	6	803
Com USP	840	14	854

According to **Figure 4.1**, the name of the five samples were described as following:

❖ Ballast Ref. (Ballast alone as reference)

❖ Para Mat (Ballast with a ballast mat using para rubber)

❖ Com. Mat (Ballast with a ballast mat using commercial product)

❖ Para USP (Ballast with an under-sleeper pad using para rubber)

❖ Com. USP (Ballast with an under-sleeper pad using commercial product)

Figure 4.1 shows the amount of total breakage of five samples. In comparison to ballast ref case, using ballast mat placed at the bottom of the ballast box with para rubber and commercial product, both cases had increased fine breakage and coarse breakage cover of 78.9% and 43%, respectively. Ballast using Para rubber and commercial product had about the same amount of percent coarse breakage with 0.46% and 0.45%, respectively. However, ballast with commercial product matt (0.11%) produced higher percentage of fine breakage than ballast with para rubber matt (0.06%).

Meanwhile, using under-sleeper pads (USP) with para rubber and the commercial product showed significant reduction in total ballast breakage in comparison to the ballast reference case. The Para USP case performed the best, with total percent breakage of 18.91% of the ballast reference case. The commercial USP performed the reduction of total breakage percentage of 61.76% of the total ballast reference case.

A possible explanation for the case of Com. Mat which had the highest ballast breakage is due to higher resilient deformation and lower resilient modulus of the ballast box, which can be seen in figure 4.18 and 4.19. Because the high settlement is the result of ballast particle arrangement, this may cause more abrasion of ballast particles.

4.1.2 Ballast breakage in each zone of ballast box

In order to study the locations of ballast breakage, the ballast particles had been marked with numbers and letters and placed in six different zones inside the box before testing. The weight of ballast particles placed in each zone were determined before the test. After the test, the ballast particles were taken out of the box, measured their weights and taken photos for image processing analysis. The ballast weight before and after the test of each particle in each zone was then determined to find the percentage of weight change by using the equation below.

$$\text{Percent weight loss in each zone} = \frac{W_{Li}}{W_{all}} \times 100 \ (\%) \qquad (4.3)$$

$$W_{Li} = W_{Bi} - W_{Ai} \qquad (4.4)$$

Where:

W_{Li} is weight loss of ballast in zone i

W_{Bi} is weight of ballast in zone i before test

W_{Ai} is weight of ballast in zone i after test

W_{all} is total weight of ballast in box before the test.
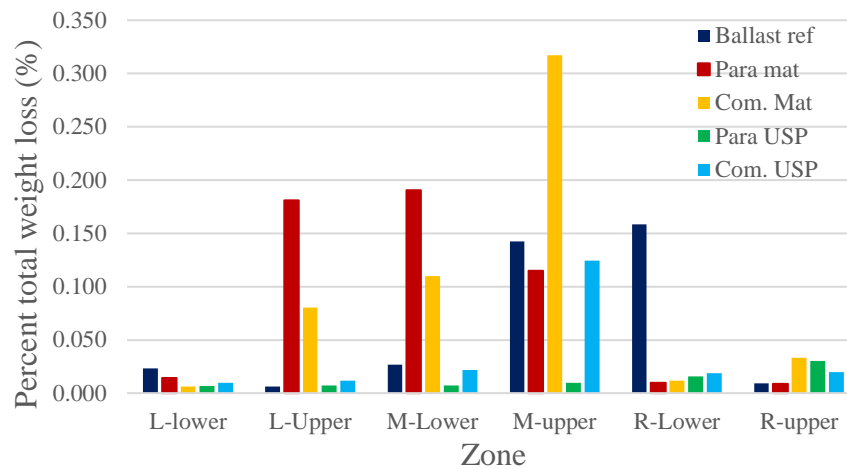
Figure 4.2 Variation of ballast breakage at different locations within the ballast box.

Figure 4.2 indicates the percentage of ballast breakage in each of the six zone locations in the box as identified earlier in Section 3.1. Although the box test had been set up symmetrically on loading position, it appeared that higher ballast breakage could take place in one side (left or right). These might happen due to the uncontrollable compaction density of ballast particles in the box during the specimen preparation. Meanwhile, the breakage amounts of upper and lower zones seem to provide some interesting information. Following evidence was observed from the graphs.

- It can be seen that Ballast ref placed at the lower zone had higher breakage percentage than those placed at the upper zone with 0.208% and 0.158%, respectively.
- For the Com. Mat and Para mat, it was found that the upper zone of both samples had the highest ballast breakage percentage with 0.431% and 0.305%, respectively. Whereas, the breakage percentage at the lower zone of both samples had the lowest breakage covers of 0.128% and 0.214%, respectively.
- The Com. USP had lower ballast breakage than ballast ref, where more breakage was observed at the upper zone than the lower zone with 0.156% and 0.05% respectively.
- The Para USP had the lowest ballast breakage compared to the breakage in the Ballast ref. The ballast breakage at the upper zone accounted for 0.047% and 0.03% for the lower zone.

Table 4.2 summary of ballast breakage in upper and lower zone

Case	Breakage in upper zones	Breakage in lower zones	Ratio of breakage upper : lower
Ballast ref	0.158%	0.208%	43:57
Para mat	0.305%	0.214%	59:41
Com. mat	0.431%	0.128%	77:23
Para USP	0.047%	0.03%	61:39
Com. USP	0.156%	0.05%	76:24

Table 4.2 shows the ratio of breakage between the upper and lower zones. Based on the results calculated, it can be summarized that the application of Com. Mat case, Para mat case, Para USP and Com. USP had more breakage in the upper zone than lower zone, in comparison to Ballast ref where more ballast breakage was found in the lower zone than the upper zone.

4.2 Ballast Particle Breakage
4.2.1 Weight changes of ballast particles.
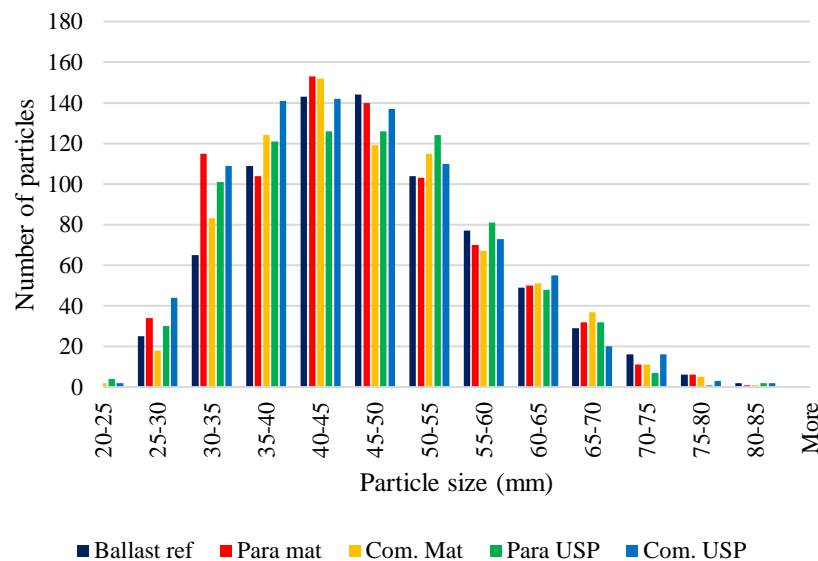
Figure 4.3 Histogram of ballast particle size of five cases

The size of each ballast particle can be determined from the width dimension using image processing technique. **Figure 4.3** shows the distribution of ballast particle sizes in each box. From the graphs, there are 13 sizes with ranges of 20-25, 25-30, 30-35, 35-40, 40-45, 45-50, 50-55, 55-60, 60-65, 65-70, 70-75, 75-80, and 80-85mm. The number of particles in five boxes is 769, 826, 785, 803, and 854 for Ballast ref, Para mat, Com. Mat, Para USP, and Com. USP, respectively. The distribution of ballast was mostly at the size of 40-45mm, while greater sizes between

80-85mm had the lowest ballast distribution. Moreover, it was found that the particle distributions of five cases were not different. Based on the trend of ballast distribution of the five samples observed in Figure 4.3 and the standard deviation of each size in all cases, which had a maximum of 1.93, it can be concluded that all samples have similar distribution.

Figure 4.4 indicates the number of particles broken into different amount of weight loss. It shows that most of particles lose their weights around 0.01-0.16g. However, there were a lower number of particles broken over 0.3g

Figure 4.5 shows the distribution of percent weight change of a particle in each box test. The percent weight change of a particle was calculated using Equation (4.5). In each graph, the sizes of particles were determined by image processing. In all graphs, most particles had percent particle breakage lower than 5%. This means that the breakage mostly occurred around the particle borders. The number of particles having percent particle breakage exceeding 5% tend to correlate with the percent ballast breakage of the box.

For those particle breakages exceeding 5%, the following evidences are observed.

- Ballast ref mostly broke at the size between 40-60mm
- Para mat broke at the size between 20-40mm
- Com. Mat seems to be breakage at the size between 40-60mm.
- The sample Para USP which had the lowest ballast breakage appears to be broken at the size of 40-60mm.
- Then the Com. USP broke at the size of 40-60mm.

$$\text{Percent weight change of a particle} = \frac{\text{weight loss of a particle}}{\text{weight of a particle before testing}} \times 100 \quad (\%) \qquad (4.5)$$
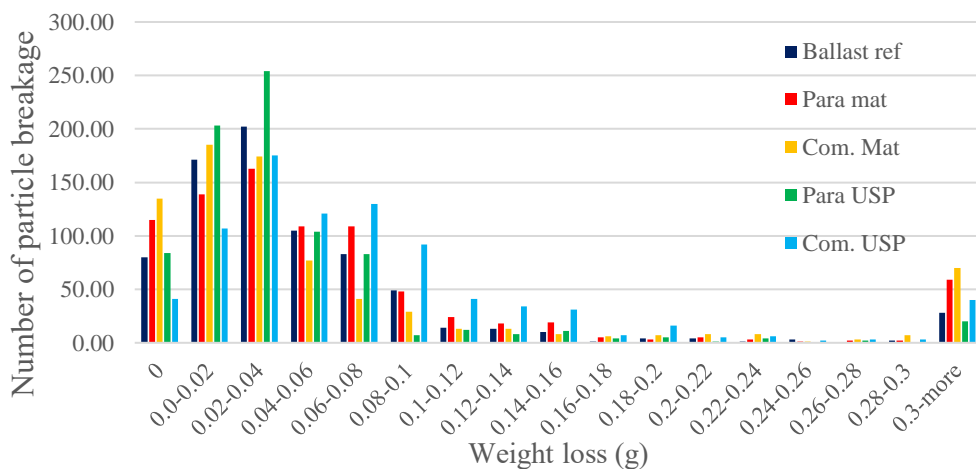
Figure 4.4 Number of ballast breakage at different weight loss.
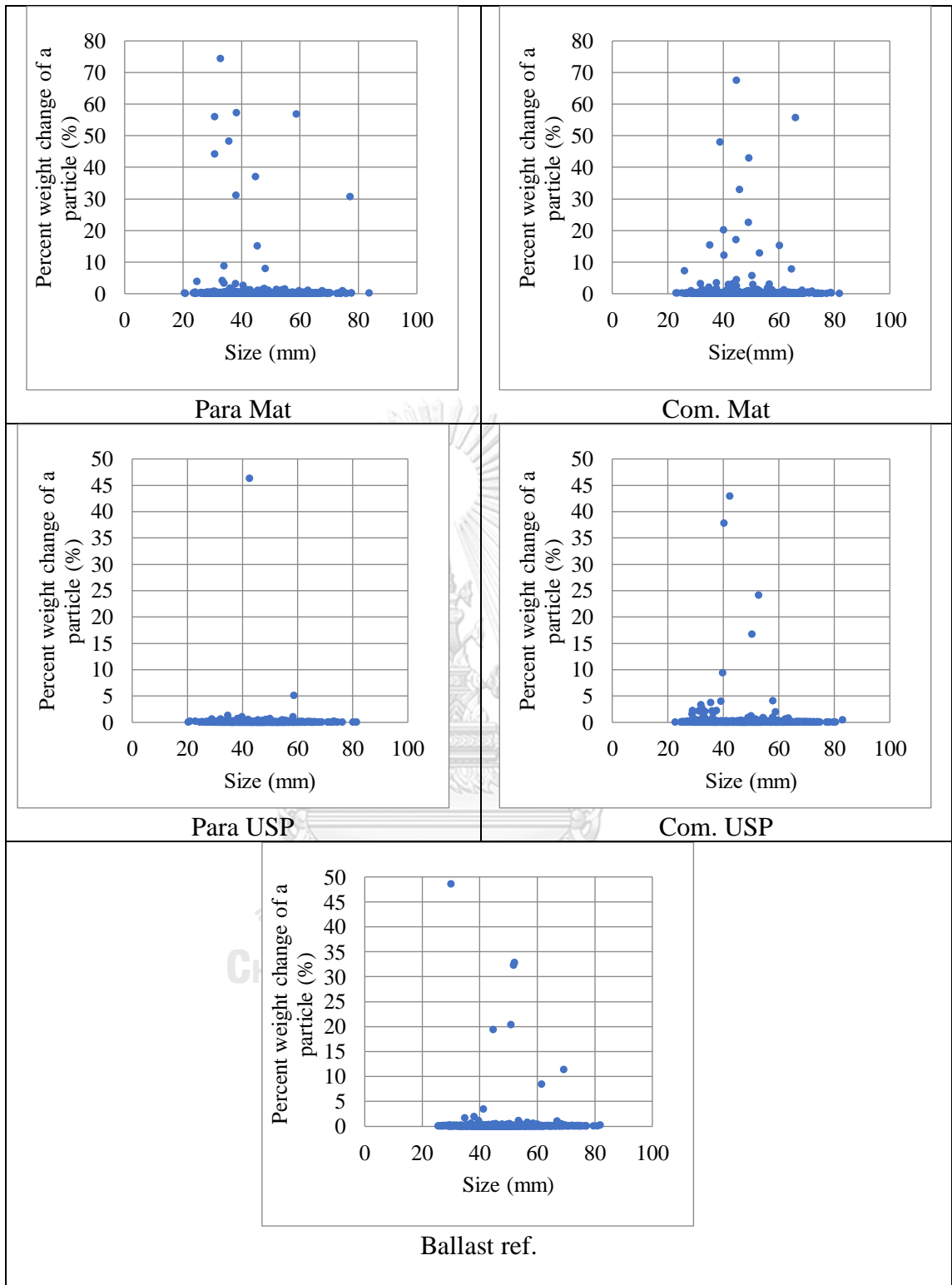
Figure 4.5 Percent weight change of a particle in each size of the five samples.
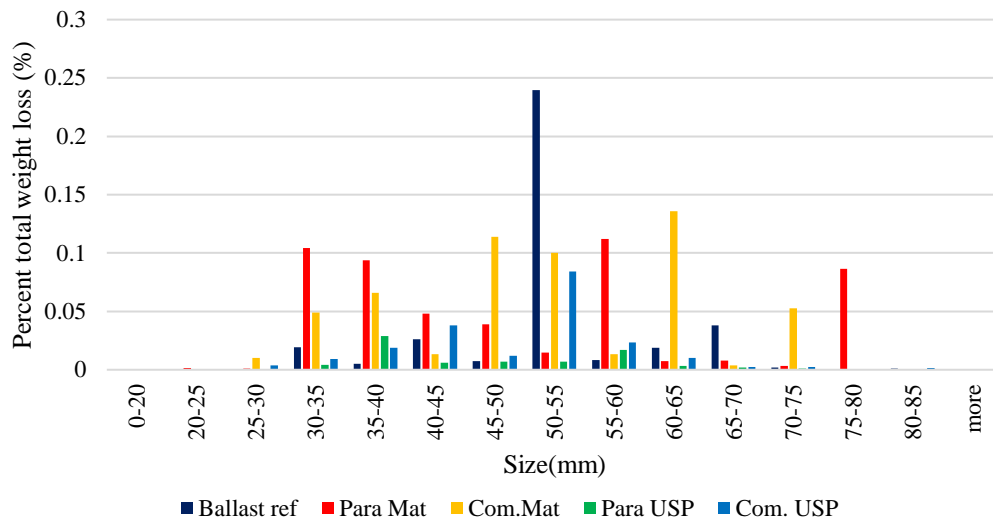
Figure 4.6 Distribution of percent weight loss in each size.

Figure 4.6 shows the distribution of total weight loss of different particles size. The total weight loss was calculated by the equation (4.6) and the size of the particles in this figure used the maximum minor axis as the particles' size. For the ballast ref case, it was observed that the highest weight loss occurred in sizes between 50-55mm, with 0.24% total weight loss. This was eight times greater than the Ballast ref with sizes between 65-70mm, which had the second highest breakage percentage, with a total wieght loss of 0.03%.

For the Para mat case, the most noticeable trend in the graph is that the total weight loss which is distributed from small to large size with a slight increase in its number of size compared to its percentage of weight loss from 30-35mm, 35-40mm, 55-60mm, and 75-80mm with 0.1%,0.09%, 0.11%, and 0.08%, respectively. In the same way, the Com. Mat case has a similar size to the Para mat in the total weight loss of each particle which range from smallest to largest size. However, most weight loss is found to be in the size that has the highest amount of particles.

Furthermore, the Com. USP has the similar trend as Ballast ref case in which the highest total weight loss is at the size between 50-55mm and then the percentage of weight loss decrease to the smaller size and bigger size.

From the graph can summarize that the breakage characteristic of Ballast ref. seems to be broken in the size that had more number of the particle. Whereas, Com. Mat and Para mat had the distribution of breakage in the smaller size to the bigger size of ballast. While Com. USP seems to be broken at the high amount of particle as Ballast ref.

$$\text{Percent total weight loss} = \frac{\text{Sum a particles weight loss of size } i}{\text{total weigth before testing}} \times 100 \qquad (4.6)$$

4.2.2 Fine particle breakage.

According to **Table 4.1**, the number of particles in the coarse breakage are quite low, so statistical analysis was conducted only on the part of fine breakage which happened in high number of particles. As mentioned in the previous section, fine breakage is defined as the broken pieces that pass 9.5 mm sieve size (3/8in.). In this section, the particles experiencing fine breakage are those with weight loss less than the highest weight of broken pieces that pass 9.5mm sieve. The particle weight loss within fine breakage of each box case is as follow.

- For the ballast ref case, the maximum weight of a particle was 1.17g. Therefore, particles with a weight loss lower than 1.17g will be considered as fine particle weight loss in this case.

- For the para rubber used as ballast mat case, the maximum weight of a particle was 1.12g. Therefore, particles with a weight loss lower than 1.12g will be considered as fine particle weight loss in this case.

- For the commercial ballast mat case, the maximum weight of a particle was 1.49g. Therefore, particles with a weight loss lower than 1.49g will be considered as fine particle weight loss in this case.

- For the para rubber used as under sleeper pad case, the maximum weight of a particle was 0.73g. Therefore, particles with a weight loss lower than 0.73g will be considered as fine particle weight loss in this case.

- For the commercial under sleeper pad case, the maximum mass of particle was 1.26g. Therefore, particles with a weight loss lower than 1.26g will be considered as fine particle weight loss in this case.

4.2.2.1 Analyze differences of fine breakage between five samples

In this section, the percentages of particle breakage in five samples are compared. One-Way ANOVA test at 95% confidence level will be used to observe if there are any statistical differences between the samples.

Table 4.4 shows the output of the ANOVA analysis and whether or not there is a statistically significant difference between the group means. If found that the significance value equals 0.000, which is less than 0.05, there is a statistically significant difference in the mean percent particle weight loss between the different samples. These results indicate that at least one pair are statistically different, but we do not know which of the specific groups are statistically different from each other. Therefore, Dunnett T3 post hoc test will be used to identify the statistical differences between each specific groups.

Table 4.5 shows multiple comparisons between the five samples which derived from the Dunnett T3 post hoc test. The Dunnett T3 post hoc test was used in this study

because differences in the variances of the five samples were observed, which can be seen in **Table 4.3** where a test of variance homogeneity showed a P-value equivalent to 0.000 (>0.05), indicating statistical significance in the samples. Therefore, the results showing which groups were statistically different from each other are as follows.

- In the Dunnett T3 test, the null hypothesis is that the particle breakage in both samples are statistically similar, while the alternative hypothesis is that the particle breakage in both samples are not statistically similar. For the comparison between the ballast ref sample and para rubber used ballast mat, there is a high statistical significance between the samples at a p-value of 0.000 (<0.05); hence, the null hypothesis can be rejected. In summary, the percentage of particle breakage in both ballast ref case and Para Mat case are statistically different at 95% confidence level.

- The ballast ref and commercial ballast mat sample was also highly statistically significant at a p-value of 0.006 (<0.05), indicating that both samples are not statistically similar. In summary, the percentage of particle breakage in both ballast ref case and commercial ballast mat case are statistically different at 95% confidence level.

- On the other hand, comparisons between sample ballast ref and para rubber used under sleeper pad showed a P-value of 1.000, which exceeded the high statistical significance level of 0.05. In this case, the null hypothesis is accpeted, meaning that the particle breakage in both samples are similar. In summary, the percentage of particle breakage in both ballast ref case and Para USP case are statistically similar at 95% confidence level.

- Finally, the comparison between sample ballast ref and commercial under sleeper pad showed a P-value of 0.000 (<0.05), indicating that the particle breakage in both samples are not similar. Therefore, the null hypothesis can be rejected. In summary, the percentage of particle breakage in both ballast ref case and Com USP case are statistically different at 95% confidence level.

Table 4.3 Test of Homogeneity of Variances

Levene Statistic	df1	df2	Sig.
19.822	4	3950	0

Table 4.4 ANOVA for five case studies

	Sum of Squares	df	Mean Square	F	Sig.
Between Groups	1.73	4	0.433	11.625	0
Within Groups	146.975	3950	0.037		
Total	148.705	3954			

Table 4.5 Multiple Comparisons for five samples

(I) 1= Ballast ref, 2=Para mat,3=Com mat, 4=Para USP,5=Com USP	(J) 1= Ballast ref, 2=Para mat,3=Com mat, 4=Para USP,5=Com USP	Mean Difference (I-J)	Std. Error	Sig.	95% Confidence Interval	
					Lower Bound	Upper Bound
1	2	-.03722*	0.00912	0	-0.0628	-0.0116
	3	-.03376*	0.00978	0.006	-0.0612	-0.0063
	4	0.00184	0.00498	1	-0.0121	0.0158
	5	-.04957*	0.00853	0	-0.0735	-0.0257
2	1	.03722*	0.00912	0	0.0116	0.0628
	3	0.00346	0.01226	1	-0.0309	0.0378
	4	.03906*	0.00891	0	0.0141	0.0641
	5	-0.01235	0.01128	0.959	-0.044	0.0193
3	1	.03376*	0.00978	0.006	0.0063	0.0612
	2	-0.00346	0.01226	1	-0.0378	0.0309
	4	.03560*	0.00958	0.002	0.0087	0.0625
	5	-0.01581	0.01182	0.864	-0.0489	0.0173
4	1	-0.00184	0.00498	1	-0.0158	0.0121
	2	-.03906*	0.00891	0	-0.0641	-0.0141
	3	-.03560*	0.00958	0.002	-0.0625	-0.0087
	5	-.05141*	0.0083	0	-0.0747	-0.0281
5	1	.04957*	0.00853	0	0.0257	0.0735
	2	0.01235	0.01128	0.959	-0.0193	0.044
	3	0.01581	0.01182	0.864	-0.0173	0.0489
	4	.05141*	0.0083	0	0.0281	0.0747

* The mean difference is significant at the 0.05 level.

4.2.3 Dimension changes of ballast particle.

$$\text{Percent change by size of major axis } = \frac{\text{Ma}_B - \text{Ma}_A}{\text{Ma}_B} \times 100 \quad (\%) \qquad (4.7)$$

$$\text{Percent change by size of minor axis } = \frac{\text{Mi}_B - \text{Mi}_A}{\text{Mi}_B} \times 100 \quad (\%) \qquad (4.8)$$

Where**:**

Ma$_B$ is the length of major axis before testing.

Ma$_A$ is the length of major axis after testing.

Mi$_B$ is the length of minor axis before testing.

Mi$_A$ is the length of minor axis after testing.

According to the results of the calculation and the graphs depicted in this section, the size of the ballasts which was analyzed by using images taken from a camera showed far too much changes and there were many particles were the change in negative percent. For example, it was found that there was an increase in some of the ballasts' size after the test, which is presumed to be an error caused by many potential factors such as the positioning of the ballast which may have moved around during or after the test; or the positioning of the camera which may have changed after the sample test. In order to know if the orientation of the particle has been changed or not, it can be compared with the weight loss of the particles that did not change too much in the before and after test. **Figure 4.7** shows the changing of particle orientation.

Major axis	Minor axis
1. Ballast ref	2.Ballast ref
1. Para mat	2. Para mat
1.Com. Mat	2.Com. Mat
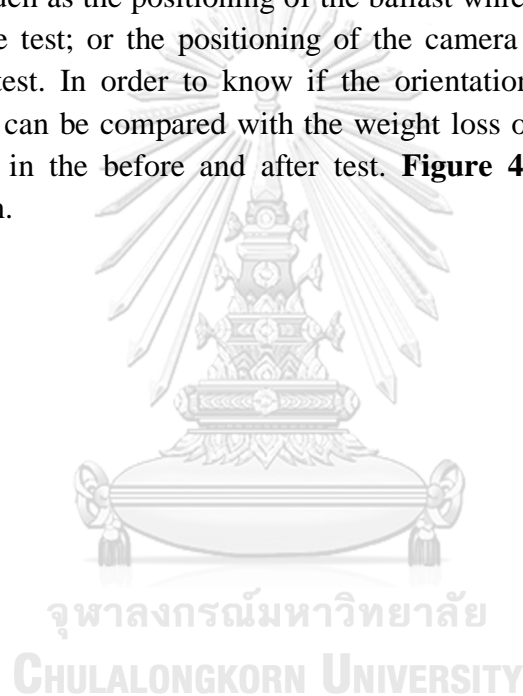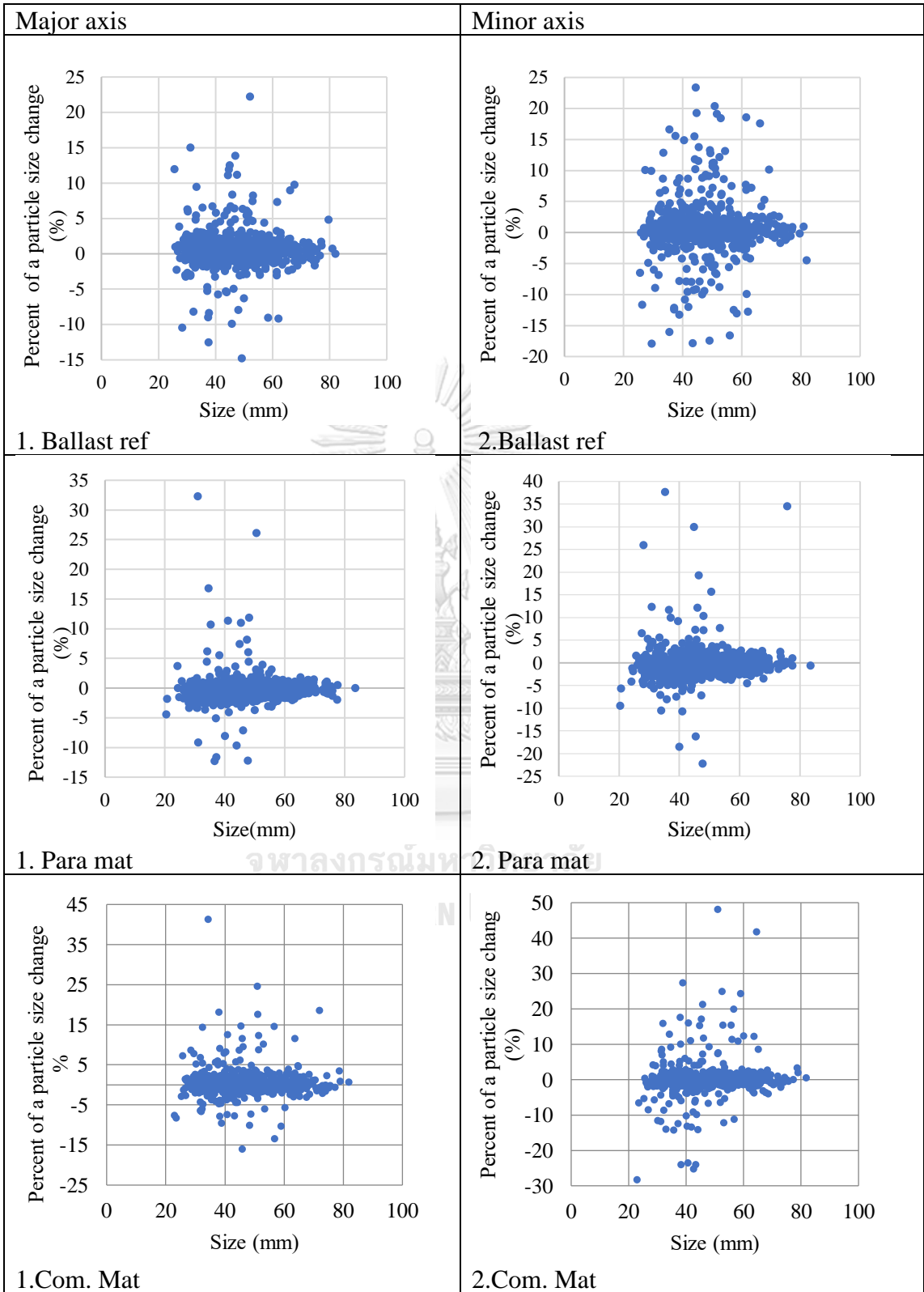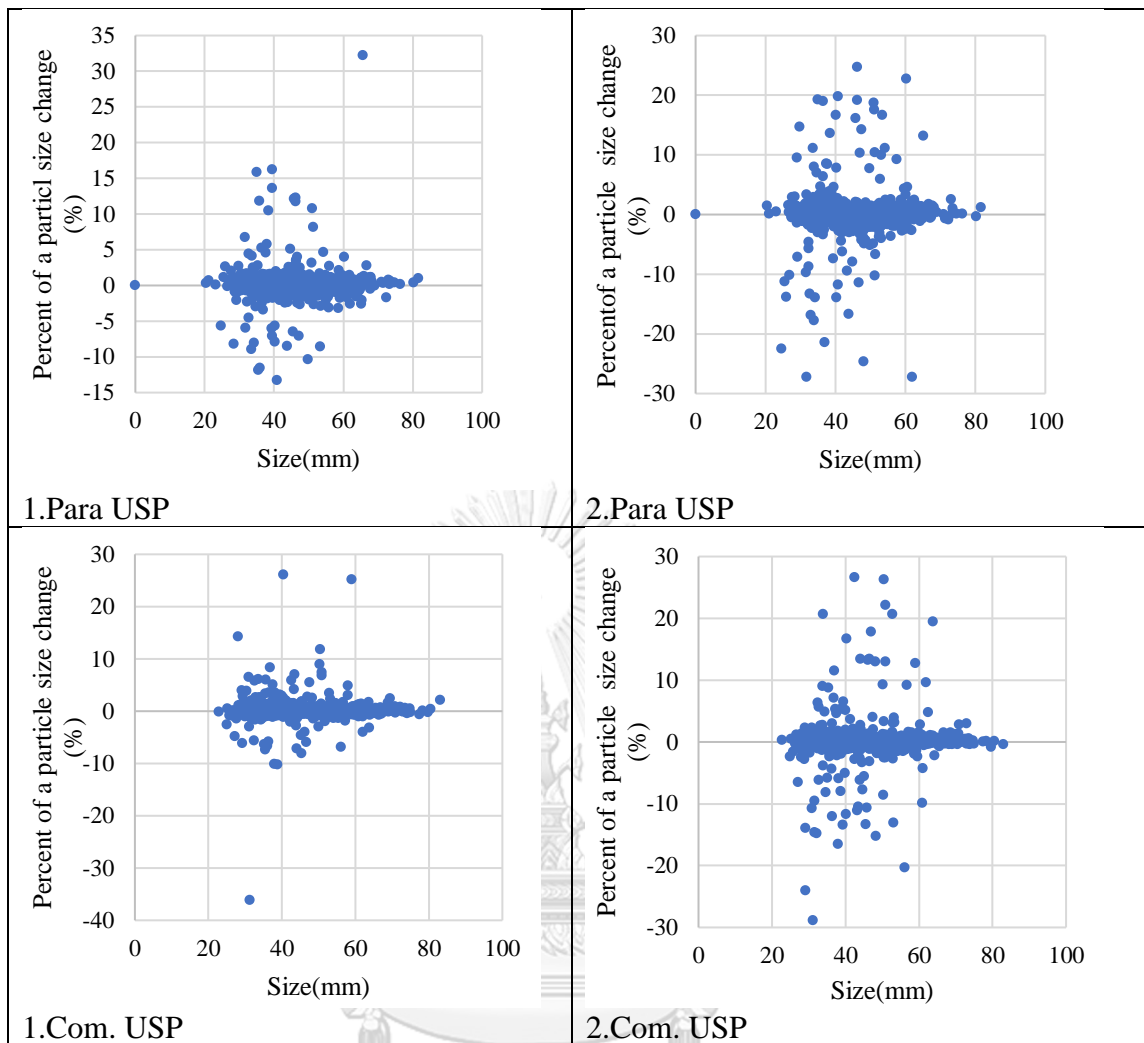
Figure 4.7 Percent particle size change of ballast of image analysis of five samples.

Image before testing	Image after testing
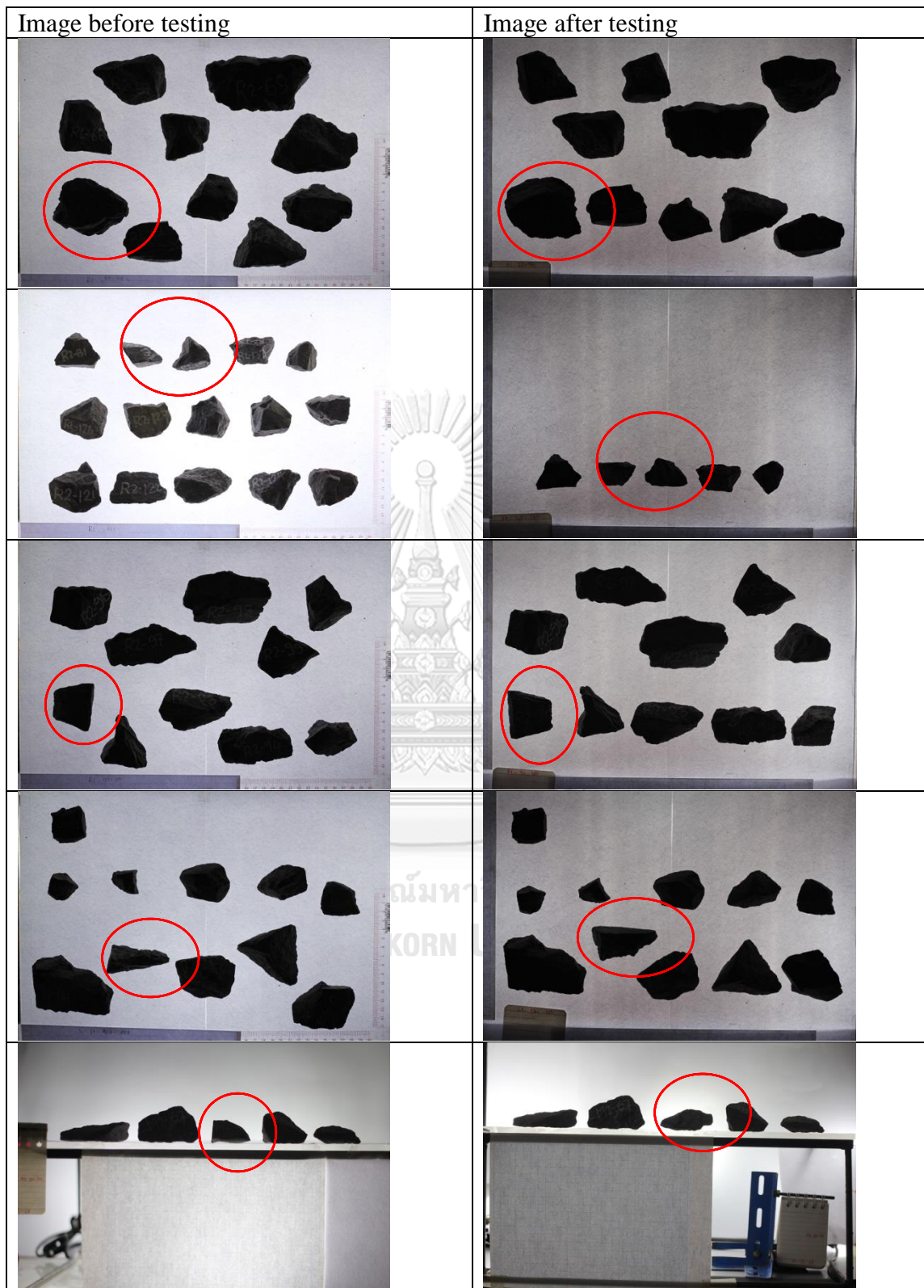
Figure 4.8 Ballast shape capture in different position before and after testing.

4.2.4 Weight change of particle by dimension ratio

The dimensional ratios of aggregation determined by the flat and elongated particles test to identify aggregation that tend to fracture easily and narrow dimension which can make aggregate more degradaded. The elongated particle means the length to the width ratio (L/W), while the flat particle implies the thickness to the width ratio (H/W). The dimension of the aggregation covers 3 parts such as width (W), length (L), and thickness (H). In order to analyze the dimensional ratios of aggregation by image processing the researcher used the maximum major axis as the length (L) of particles, the maximum minor is the width (W), and the minimum minor is the thickness (H).

4.2.4.1 Weight change of particle by L/W ratio.
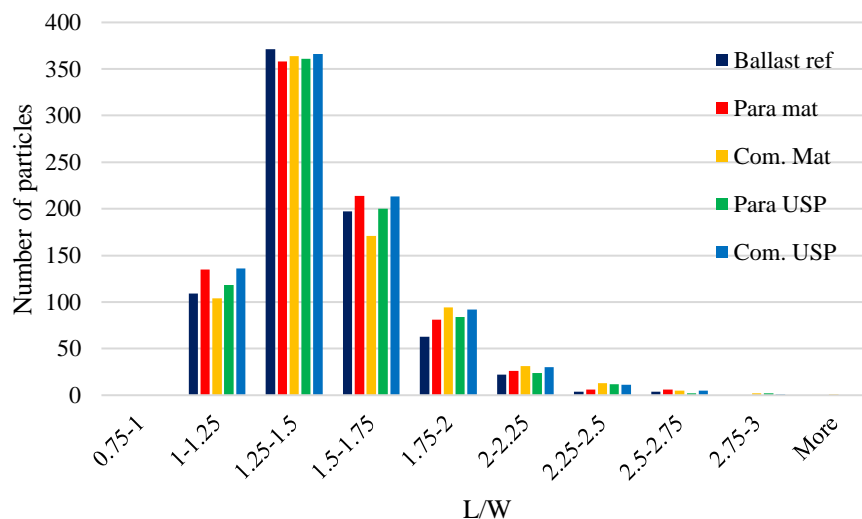
Figure 4.9 Distribution of ballast in each L/W ratio of all samples

Figure 4.9 shows the distribution of particles in each L/W ratio. The number of particles is distributing in the range of 1-1.25, 1.25-1.5, 1.5-175, 1.75-2, 2-2.25, and 2.5-2.75. It can be seen that most of the particles are at the ratio of 1.25-1.5 for Ballast ref, Para mar, Com. Mat, Para USP, and Com. USP samples, with the amount of 371, 358, 364, 361, and 366 respectively. The second highest amount is at the ratio of 1.5-1.75 in which the Ballast ref case, Para mar case, Com. Mat case, Para USP case, and Com. USP case has the respective amount of 197, 214, 171, 200, 213 particles. The ratio of 1-1.25 in each sample of Ballast ref, Para mar, Com. Mat, Para USP, and Com. USP had the number of 109, 135, 104, 118, 136. While the ratio of 1.75-2 in each sample of Ballast ref, Para mar, Com. Mat, Para USP, and Com. USP had the number of 63, 81, 94, 84, and 30. The number of particles in all samples

decreased from the ratio of 2 to the ratio of 2.75. In summary, the number of particles in each L/W ratio of all cases have similar trend distribution.
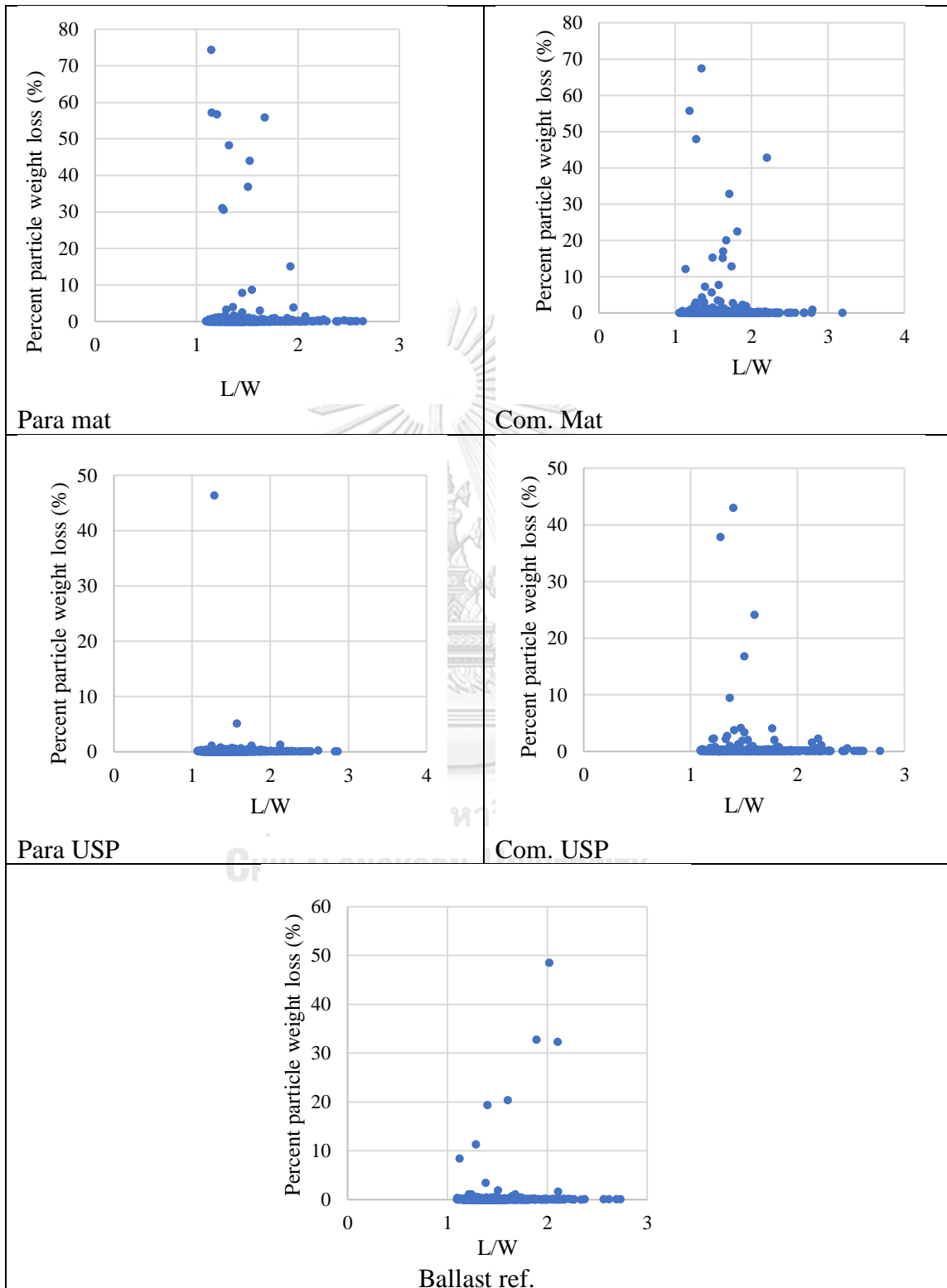
Figure 4.10 Percent a particle weight change of L/W ratio.

Figure 4.10 shows the changing of a particle weight in percent against the L/W ratio. The percent weight loss of a particle was calculated from equation (4.5). According to the graphs above, we can see that all samples had different distribution of particle weight loss in each ratio. All samples were broken into ratios around 1-2 and broke into sizes that had more amounts.

Figure 4.11 shows the percentage of total weight loss distribution in each L/W ratio. The percent weight loss in this graph was calculated by using the equation (4.9). The data from image processing was used as the dimension of the particle to define the L/W ratio. The particles in all of the five samples were separated into ratios of 8 ranges such as 1-1.25, 1.25-1.5, 1.5-1.75, 1.75-2, 2-2.25, 2.25-2.5, 2.5-2.75, and 2.75-3. The most obvious trend of Ballast ref case in the graph is that the percentage of total weight loss of ratio at the range of 2-2.25 is higher than the percentage of weight loss of ratio from 1.25-2.

On the other hand, the trend of Para mat had the highest amount of weight loss at the range of 1-1.25, with a percentage of weight loss decreasing from 1.25 to 2.5 L/W ratio. Similarly, ballast using Com. Mat, had the highest amount of total weight loss at the range of 1.25-1.5. Most of its particle loss weight around the range of 1-1.75 L/W ratio, with the amount of weight loss decreasing from small ratio to the bigger ratio.

Furthermore, the total weight loss of Com USP has the highest percentage at the range of 1.5-1.75 and the second highest is in the range of 1.25-1.75. Likewise, the Para USP has the highest weight loss at the range between 1.25-1.5 and the second is at the range of 1.5-1.75. Both cases have similar weight loss, with most weight at the ratio between 1.25 -1.75 where there are the highest number of particles.

In conclusion, the use of para rubber and commercial material placed under ballast layer caused the breakage of particle mostly break in the less L/W ratio, while the para rubber and commercial used as under sleeper pad mostly breakage the ratio that had the high amount of particles.

$$\text{Percent weight loss of ratio i} = \frac{\text{Sum weight loss of particle ratio i}}{\text{Total weight before testing}} \qquad (4.9)$$
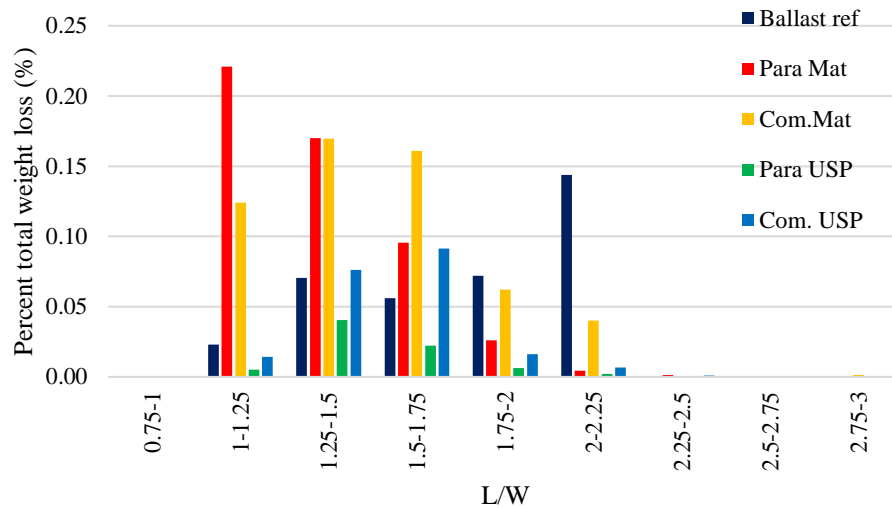
Figure 4.11 percent frequency ballast breakage by weight loss in each L/W ratio.

$$\text{Percent weight loss of a particle} = \frac{\text{Sum weight loss of particle at ratio } i}{\text{Sum weight of particle at ratio } i} \times 100 \qquad (4.10)$$
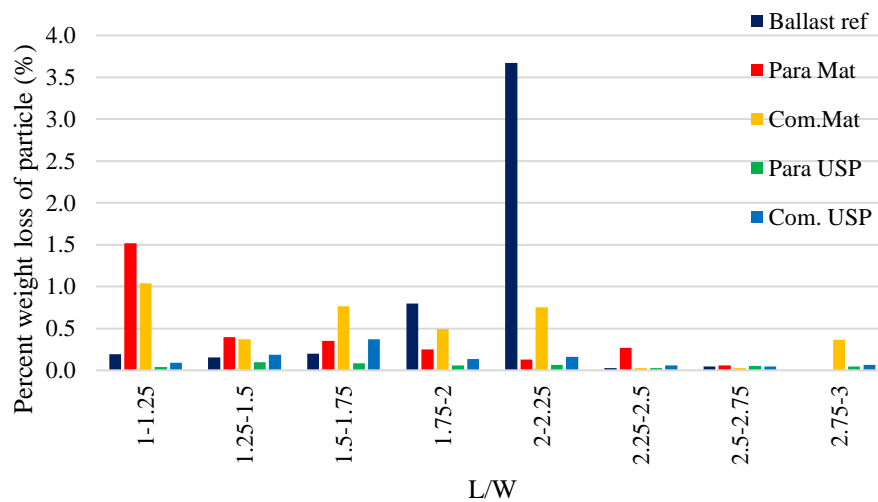
Figure 4.12 particle weight loss by L/W ratio.

    Figure 4.12 indicates the percent weight loss of a particle in each ratio. The percentage of particle weight loss was calculated by the equation (4.10). The particle in all five sample were separated into 8 ranges of ratios such as 1-1.25, 1.25-1.5, 1.5-1.75, 1.75-2, 2-2.25, 2.25-2.5, 2.5-2.75, and 2.75-3. Based on the comparisons of ballast breakage in each range of L/W ratio, it can be found that both Com. Mat and Para mat had the highest ballast breakage at the range of 1-1.25, 1.25-1.5, 1.5-1.75, 2.25-2.5 which means that both materials used as ballast mat increase the ballast

breakage in the low elongation. Moreover, the percentage of ballast breakage of both samples was close together in any range of L/W ratio. The ballast breakage rate in Ballast ref sample was greater than the Com. Mat and Para mat sample only in the range of 1.75-2 and 2-2.25. In contrast, Para USP and Com USP tend to have lower ballast breakage than Ballast ref. in most of the range. Although ballast breakage percentage in Com USP sample with ranges between 1.5 and 1.75 L/W ratio was greater than that of Ballast ref, both Para USP and Com USP, overall, decrease ballast breakage.

4.2.4.2 Percent weight change by ration H/W
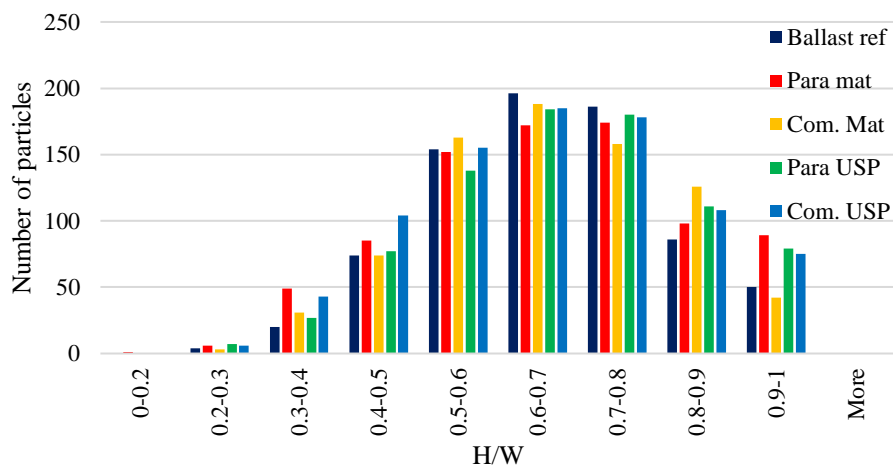
Figure 4.13 Distribution of ballast in each H/W ratio of all samples

Figure 4.13 shows the distribution of particles in each H/W ratio of all five samples. The number of particles was distributed in the range of 0.2-0.3, 0.3-0.4, 0.4-0.5, 0.5-0.6, 0.6-0.7, 0.7-0.8, 0.8-0.9, and 0.9-1. According to the chart, the highest amount of the particle was at the range of 0.6-0.9 H/W ratio with 196, 172, 188, 184, and 185 particles of sample Ballast ref, Para mar, Com. Mat, Para USP, and Com. USP respectively. Around 70% of particles are in the range between 0.5-0.8 H/W ratio. The lowest number of particles is at the range of 0.2-0.3 H/W ratio. Lastly, the trend of particle distribution in each range of ratio is not different.

Figure 4.14 shows the distribution of percent weight change of a particle in H/W ratio. The percent weight change of a particle was calculated using Equation (4.5). In this part, the H/W ratio means the flatness of particles by using the thickness (H) as the minimum minor axis, and the width (W) is the maximum minor axis from image analysis. For those particle breakages exceeding 5%, the following evidence were observed.

- Ballast ref mostly broke at the ratio between 0.6-0.8.
- Para mat broke at the ratio between 0.4-0.8.

- Com. Mat sample seems to be broken at the ratio between 0.4-1.
- The sample Para USP which had the lowest ballast breakage appears to be broken at the ratio of 0.7-0.8.
- Then the Com. USP broke at the ratio of 0.3-0.9.
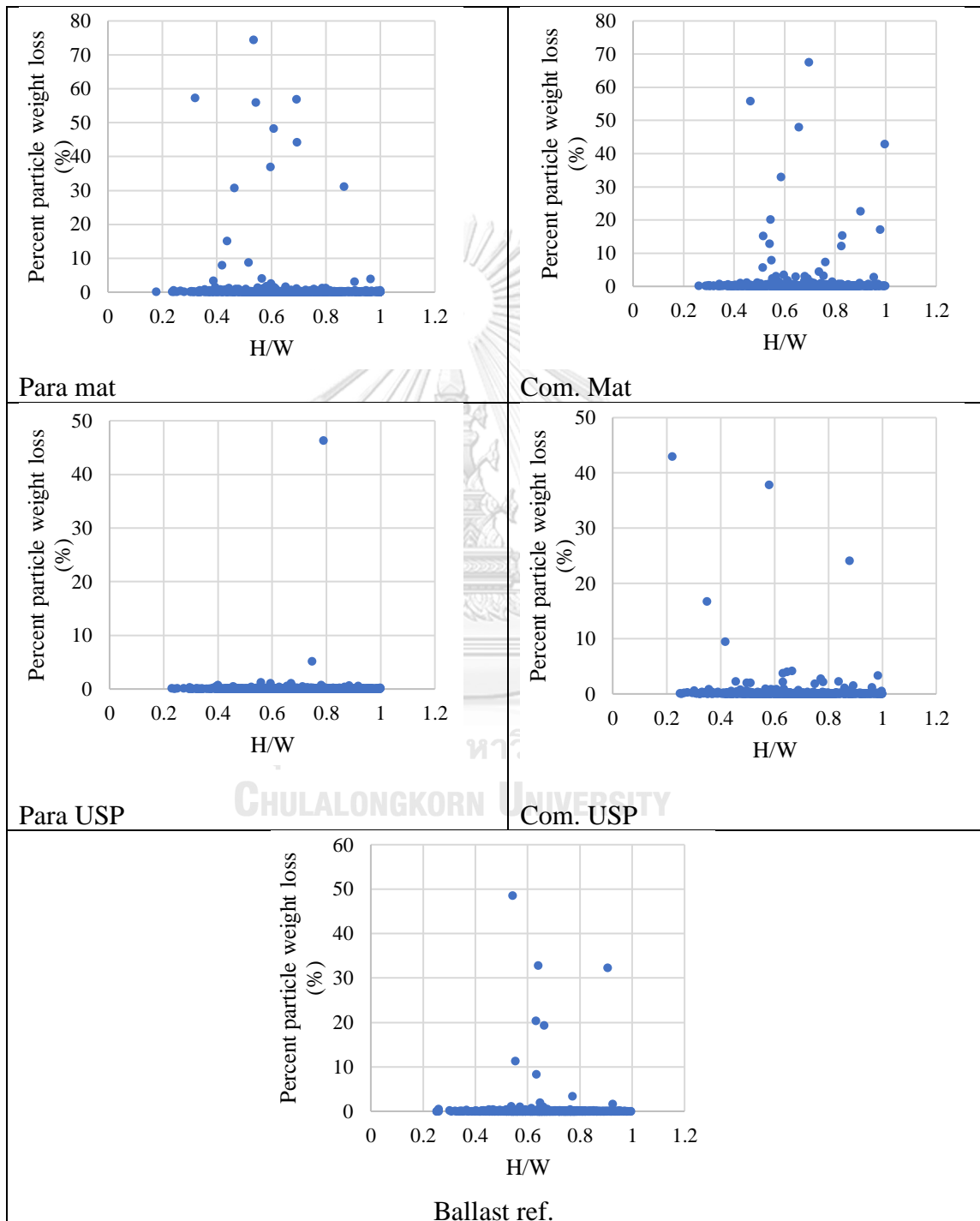
Figure 4.14 Percent weight loss of a particle by H/W ratio.
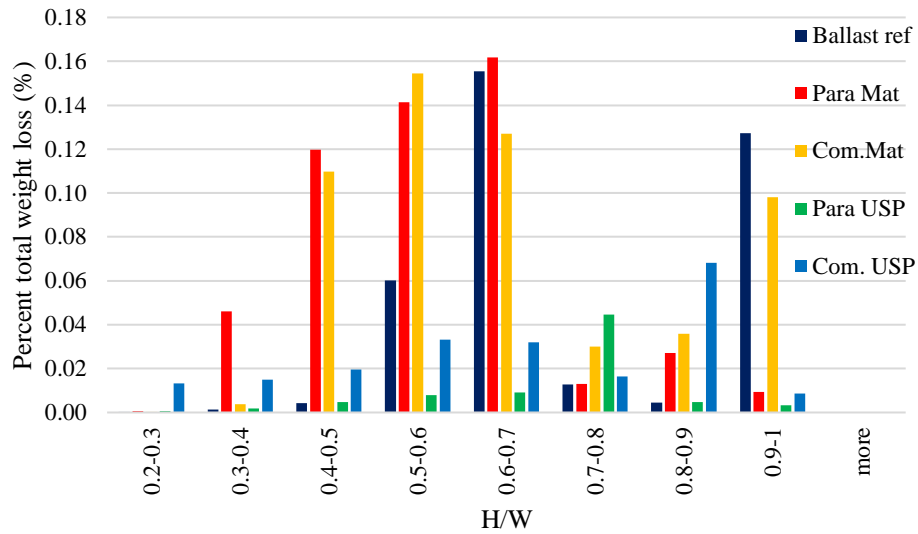
Figure 4.15 Percent total weight loss in each ratio H/W

Figure 4.15 shows the distribution of the total weight change in the different range of H/W ratio. The percentage of total weight loss in this graph was calculated by using the equation (4.11). The range of H/W ratio in this study was separated into 8 range such as 0.2-0.3, 0.3-0.4, 0.4-0.5, 0.5-0.6, 0.6-0.7, 0.7-0.8, 0.8-0.9, and 0.9-1. From the chart, it is clear that Ballast ref had the highest weight loss at the range of 0.6-0.7, with a total weight loss percentage of 0.19%, while the second highest weight loss was observed at the range of 0.9-1, with 0.13% of total weight loss.

For Para Mat case and Com Mat, the total weight loss percentage was mostly observed in the range of H/W ratio between 0.6-0.7 to 0.3-0.4. For Com Mat samples, a high percentage of ballast weight loss was found in the H/W ratio range of 0.9-1.

Furthermore, the Para USP had the highest total weight loss percentage at the H/W ration range of 0.7-0.8 (0.04% total weight loss) and the percentage of total weight loss in other range seem to be close together. Similarly, the Com USP had the highest percentage of total weight loss at the range of 0.8-0.9 (0.07% total weight loss), and the amount of breakage in these samples distribute to another ratio with similar percentages.

In conclusion, the use of Para rubber and commercial material cause the total weight loss to distribute the H/W lower than 0.7, while the used of para rubber and commercial material as under sleeper pad cause the breakage to distribute to all range ratio and the percentage seem to be firmly together.

$$\text{Percent weight loss} = \frac{\text{sum weight loss of a particle in } i \text{ ratio}}{\text{weight before testing of sample}} \times 100 \qquad (4.11)$$
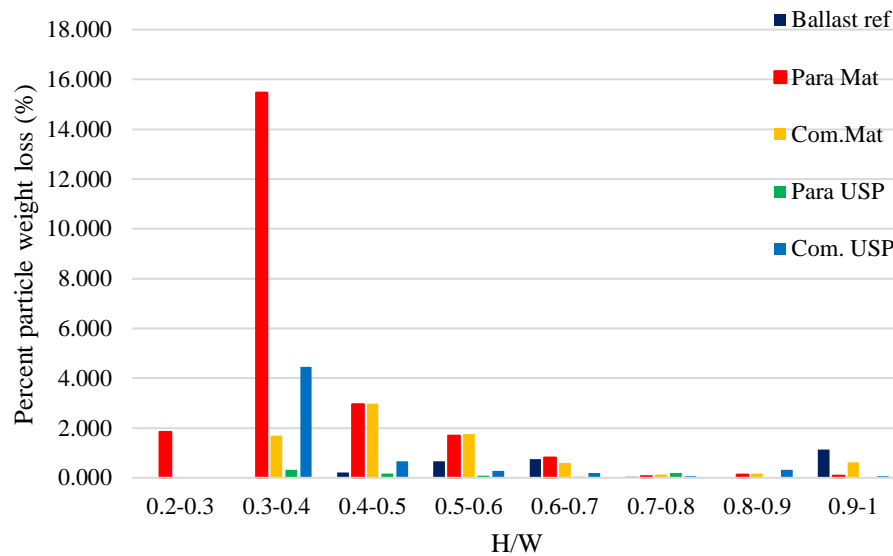
Figure 4.16 Percent weight loss by ballast H/W ratio.

Figure 4.16 shows percent weight loss of particle in each H/W ratio. The percent weight loss was calculated by using the equation (4.10) to study the weight loss of particle in the same H/W ratio of all samples. Based on the chart, it can be seen that the Para Mat case has the highest percentage of particle weight loss at the range 0.3-0.4, with 15.56% of particle weight loss. This was three times more than the weight loss of Com USP, which has the second highest weight loss percentile. Moreover, the percent weight loss in any range of Para Mat and Com Mat have higher amount of percent weight loss than Ballast ref case except the range of 0.6-0.7 and 0.9-0.1. Likewise, the use of Com USP increases the ballast breakage at the ratio of 0.3-0.4 and 0.4-0.5 compared with the ballast ref.

From the comparison of five samples in each range of H/W ratio, it was found that the percent weight loss of Com. Mat and Para mat seemed to be higher than Ballast ref in any range of H/W ratio. Moreover, the number of particles in 0.3-0.4, 0.4-0.5, and 0.5-0.6 had lower number of particles, but there was a high ballast breakage which means that elastic material has an effect on the low flatness particles in comparison of ballast ref.

$$\text{Percent weight loss by ballast size} = \frac{\text{Sum weight loss of particle at ratio } i}{\text{Sum weight of particle at ratio } i} \times 100 \qquad (4.12)$$

4.2.4.3 Weight change of ballast by H/L ratio
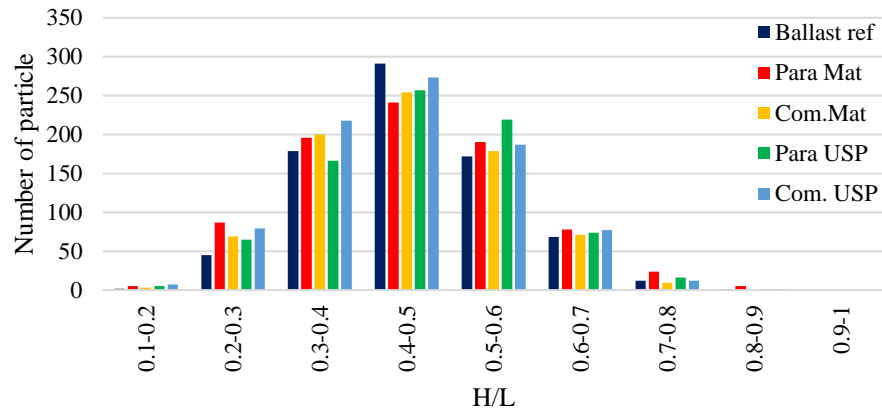
Figure 4.17 Distribution of ballast particle in each H/L ratio.

Figure 4.17 shows the distribution of particles of all five samples. In this chart, the range of H/L ratio was separated into 8 ranges namely, 0.1-0.2, 0.2-0.3, 0.3-0.4, 0.4-0.5, 0.5-0.6, 0.6-0.7, 0.7-0.8, and 0.8-0.9. It can be found that most of the particles were at the range of 0.4-0.5 H/L ratio in the amount of 291, 241, 254, 257, and 278 particles for Ballast ref, Para mar, Com. Mat, Para USP, and Com. USP, respectively. For the range 0.3-0.4 and 0.5-0.6 of all samples tend to have similar amount of particles with an average of 191.8 and 189.4 particles, respectively. Likewise, the samples in the H/L ratio of 0.2-0.3 and 0.6-0.7 have an average of 69 and 73.6 particles, respectively. In addition, the range of 0.7-0.9 covers 14 particles in average. As shown in figure 4.17, approximately 70% of the number of particles in all samples in the H/L ratio were between 0.3-0.6, while about 30% are in the H/L ratio between 0.1-0.3 and 0.6-0.9. Moreover, the trend of number particles distribution has a similar amount of ballast particles in each H/L ratio.
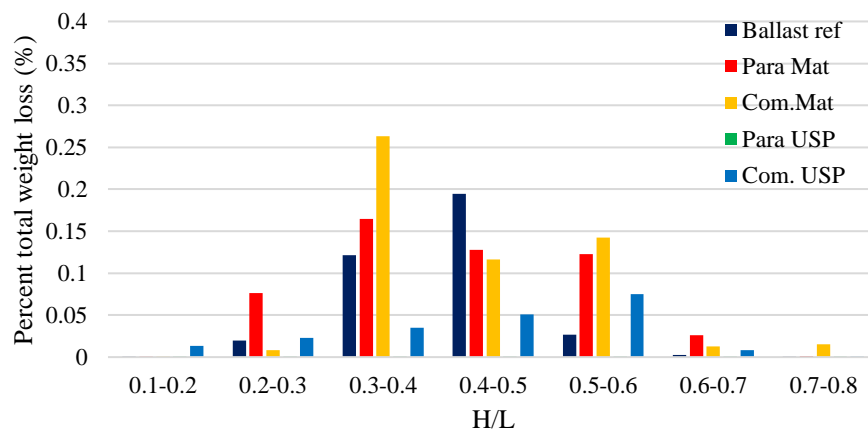
Figure 4.18 Percent weight loss by ballast H/L ratio

Figure 4.18 displays the distribution of the total weight change in different ranges of H/L ratio. For the percent of total weight loss in this graph, the researcher used the equation (4.11). In this section of H/L ratio was separated into 7 range including 0.1-0.2, 0.2-0.3, 0.3-0.4, 0.4-0.5, 0.5-0.6, 0.6-0.7, and 0.7-0.8. As shown in Figure 4.18, the percentage of weight loss of Para Mat case is distributed between 0.2-0.7 where the highest weight loss is between 0.3-0.4 with 0.16%. Similarly, the Com Mat has the highest total weight loss at the H/L ratio between 0.3-0.4 in which most of its weight loss is distributed within the range of 0.3-0.6 H/L ratio. For the Com. USP, the highest total weight loss particles are between the 0.5-0.6 H/L ratio, with 0.07% of weight loss. Whereas the percentage of weight loss decrease at the range between 0.5-0.1.

From the distribution of weight changes in each sample, it can be summarized that the ballast ref broke in high amounts of particle. In contrast, the cracking of particles in the sample Com. Mat and Para mat seems to be scattered in every H/L ratio.
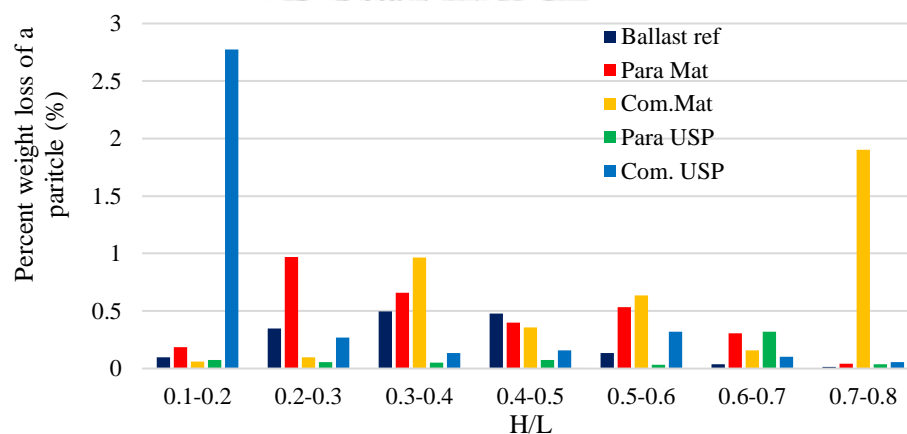
Figure 4.19 Percent particle weight loss by H/L ratio

Figure 4.19 illustrates the percent weight loss of a particle in each H/L ratio. The percent weight loss was calculated by using the equation (4.10) to study the weight loss of the particle in the same H/L ratio of all samples. According to the chart, it was found that using commercial material as under sleeper pads increases the breakage of the particle in the range between 0.1-0.2 with 2.77% weight loss. Moreover, the use of commercial material placed under ballast layer also increases the particle breakage between 0.7-0.8 H/L ratio of particles. For the Para USP, the use of para rubber can decrease the ballast breakage in any H/L ratio except in the range between 0.6-0.7 where the percentage of particle weight loss was higher than the Ballast ref by 90%.

From the results, it can be observed that the use of para rubber as a ballast mat resulted in higher ballast breakage percentage than the ballast ref in all of the H/L ratio, with an exception for the H/L ratio range of 0.5-0.6. Likewise, the use of

commercial ballast mat had the highest percentage of particle breakage in the H/L ratio range of 0.3-0.8, where there were greater numbers of particles which were quite similar in sizes. For the sample Com. USP, the highest percent weight loss of particles was observed in the 0.1-0.2 range of H/L ratio because of the weight loss also high and the number of particles quite less.

4.3 Ballast Displacement
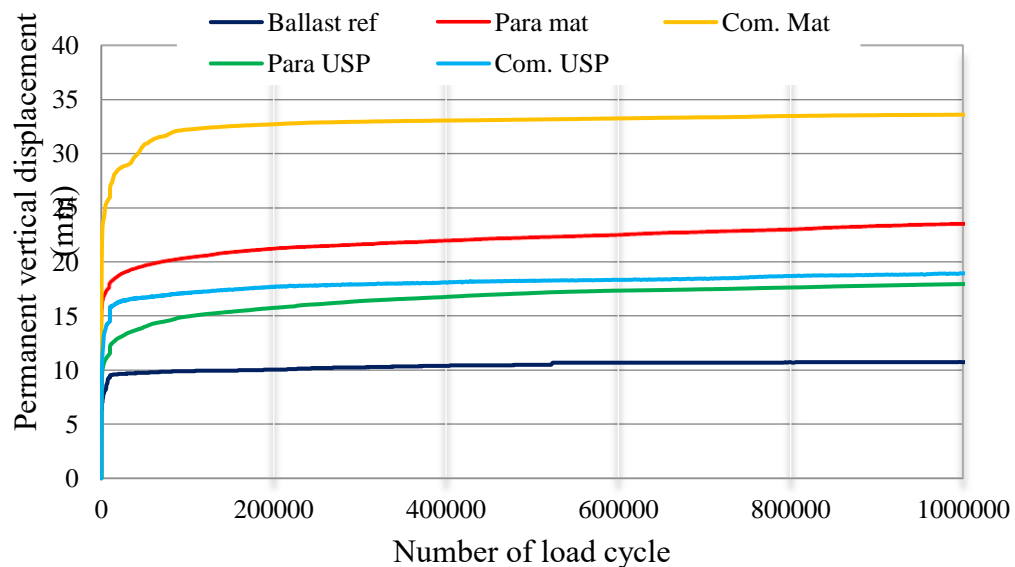
Figure 4.20 the permanent vertical displacement against number of cycles of the different ballast box condition.

The sleeper settlement is one of the most critical parameters that define the performance of the track structure. In the box test, the sleeper settlement is defined as the cumulative permanent vertical displacement of the sleeper. **Figure 4.20** shows the sleeper settlement records of the five cases. During the 10,000 cycles of preloading for all samples, there is high rate of permanent settlement increment which causes sliding and rearrangement of ballast particles in the box. After that, the permanent settlement increases at a lower rate. And the permanent settlement of the ballast ref case slightly rises after the 10,000 cycles. It illustrates that the uses of elastic material including para rubber and commercial product have resulted in higher sleeper settlement than the ballast reference case. The Com. Mat case has the highest sleeper settlement while the ballast ref case produces the least settlement. It is also clearly shown that using elastic material placed under the ballast layer causes higher settlement than using elastic material under the sleeper.

The permanent displacement rate refers to the difference between the settlement of a recorded cycle and the settlement of the next recorded cycle divided by the number of cycles between the two points. **Figure 4.21** shows permanent

displacement rate of each configurations testing. It illustrates that the sleeper tends to be stable after 100,000 cycles for all conditions.

$$\text{Permanent displacement rate} = \frac{D_a - D_b}{N_{a-b}} \tag{4.13}$$

Where;
D_a is the deformation at a cycle.
D_b is the deformation at b cycle.
N_{a-b} is number of cycle from $a - b$.
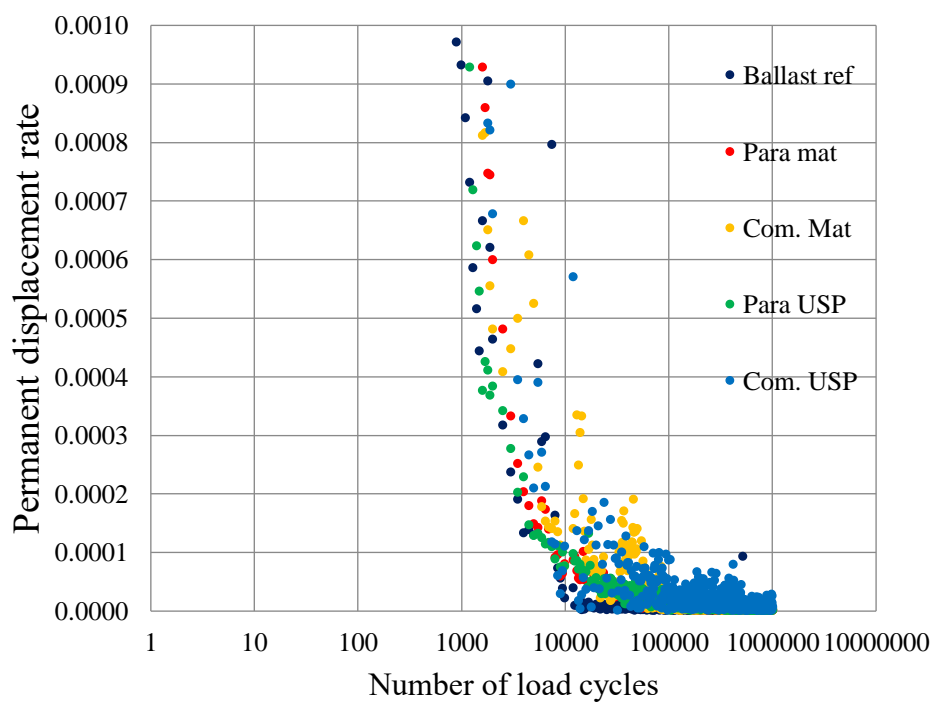
Figure 4.21 Permanent displacement rate of the different test configurations.

4.4 Resilient Deformation and Modulus of Ballast Box Reaction (k_B)
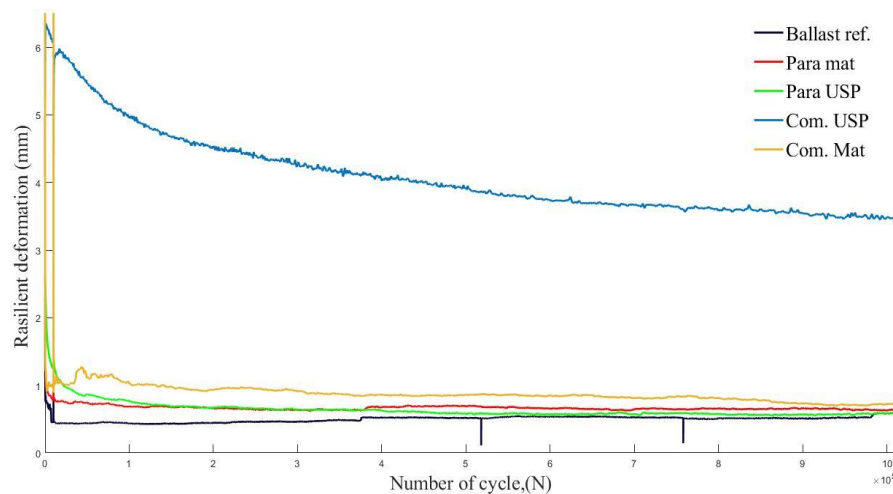
Figure 4.22 The resilient deformation from ballast box test.

$$\text{Resilient deformation} = \Delta_{\text{up-peak}} - \Delta_{\text{low-peak}} \qquad (4.14)$$

Where:

$\Delta_{\text{up-peak}}$ is the deformation while the load reach to the highest.

$\Delta_{\text{low-peak}}$ is the deformation while the load reach to the lowest.

The resilient displacement of the sleeper is calculated by using Equation (4.14). It is the recoverable displacement within a cycle of repeated load application. The resilient displacement of the sleeper in each case is plotted in **Figure 4.22**. As can be seen on the graph, all samples showed a decrease in the resilient displacement immediately at their first 10,000 cycles. After that the rate of changing in resilient displacement appears to be slower, with an exception for the Com USP sample which appears to have a different resilient displacement behavior. The trend of its resilient displacement does not decrease immediately, but it decreases slowly from the establishment until the end of testing.

Moreover, it can be seen that Com. USP had the highest resilient displacement at the first load cycle, but continues to decrease when the number of load cycle increases. Nonetheless, at the end of the test, Com. USP still had the highest resilient deformation. High resilient deformation in the Com. USP can cause high deformation and instability on the tracks and cause unsmooth track surface. High resilient deformation can also cause low track modulus which is not suitable for railway track structures because it increases stress in the rail. As a result, this may lead to wearing of rails; thus, incurring high maintenance cost and affecting train operation. On the other hand, para USP, Com. Mat and Para mat samples had resilient displacements

similar to that of the ballast ref sample, which is the better sign of using elastic materials comparing with ballast ref.
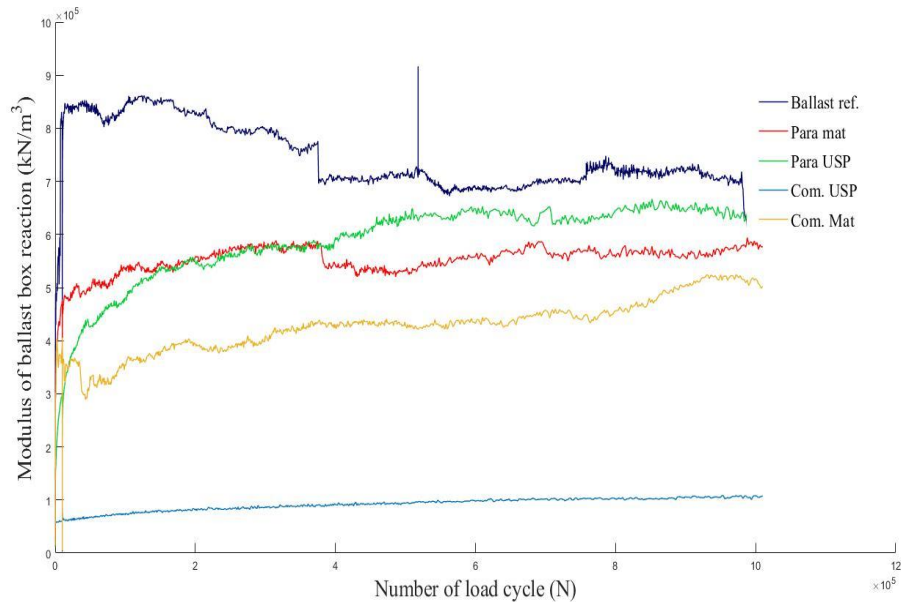
Figure 4.23 modulus of ballast box reaction against number of load cycle.

$$k_B = \frac{\frac{P}{A}}{\Delta_{up-peak} - \Delta_{low-peak}}$$
(4.15)

Where:
k_B is modulus of ballast box reaction (N/m³)
P is load (kN)
A is area of underneath sleeper (m²)
$\Delta_{up-peak}$ is the deformation while the load reach to the highest (m).
$\Delta_{low-peak}$ is the deformation while the load reach to the lowest (m).

The modulus of ballast box reaction is defined as the pressure under sleeper per unit of resilient displacement. **Figure 4.23** displays the result of the modulus of ballast box reaction against the number of load cycle recorded during ballast box tests. It can be seen that the ballast ref. had the highest track modulus and was more different from other samples. In contrast, the track modulus of Com. USP had the lowest ballast box reaction. The modulus of para mat case increases during the first 200,000 cycles. However, from 200,000 to 400,000 cycles it decreases and then remains stable until 1 million cycles. The modulus of ballast box reaction of Para USP case tends to increase with increasing number of load cycles. At 1 million cycles, its modulus is close to the track modulus of ballast ref. case.

4.5 Summary of Discussion

Based on the results of the box tests and the comparison of the results in all test conditions with the ballast ref by cyclic load, it was found that the use of para rubber and commercial product as under sleeper pads led to decreasing ballast breakage. The results in this study was consistent with (Hunt and WINKLER, 1997; Lundqvist and Dahlberg, 2005) who suggested that using elastic under sleeper pad could reduce the breakage of particles. It is also similar to the findings of (Navaratnarajah and Indraratna, 2017) who conducted a field study about using under sleeper pad with the thickness of 8mm and found that it could reduce ballast breakage. On the other hand, the result of this study is different from (Navaratnarajah and Indraratna, 2017) who used rubber mats (10 mm thickness) place beneath the ballast layer. They found that rubber mat was capable of reducing ballast breakage by about 35-45%.

In regards to the breakage of ballast particles in each zone, this study found that the breakage of ballast ref case showed a different trend in the results, compared to those found in a similar study conducted by (Navaratnarajah and Indraratna, 2017), where the highest breakage was at the top layer followed by the middle and bottom layers since there was high stress in the top layer. However, the findings in this study was similar to that of (Navaratnarajah and Indraratna, 2017)'s study when para rubber and commercial material placed under ballast layer and used as an under sleeper showed greater ballast breakage in the upper zone than the lower zone.

The results indicate that para rubber and commercial material used as ballast mat increase the overall deformation of ballast when placed on top of the stiff base, but there is only para rubber used as USP was close to the ballast ref the most. As expected, and as reported by other researchers (Miguel Sol-Sánchez et al., 2015; Navaratnarajah and Indraratna, 2017), the thickness, stiffness, and density of rubber are crucial factors in reducing the vibration and deformation in ballast. The deformation of ballast has high rate up to 10,000 load cycle cause of the ballast in these periods sliding and being rearranged within the ballast mass, and also the contribution from the abrasion and attrition of sharp angular cornered aggregates. When the load cycle loading reached around 100,000 cycles, the rate of settlement remained stable with an almost constant settlement which shows the good long-term behavior of the ballast. This study has a similar trend of settlement characteristic with other research works (Miguel Sol-Sánchez et al., 2015; Navaratnarajah and Indraratna, 2017). However, other works using rubber mat with the thickness of 10mm placed under ballast layer found that it was capable of reducing the ballast deformation. Therefore, the use of para rubber is appropriate for being used as an under-sleeper pad element the most. Although it did not reduce the sleeper settlement, it was close to the ballast ref than other material conditions.

Regarding the modulus of ballast box reaction, this study found that using para rubber as under sleeper pad had the trend closest to the ballast ref case. Other researches (Kennedy, 2011; S

ol-Sánchez et al., 2014) found that low track stiffness results in flexible track with poor deformation and ballast abrasion due to ballast flexural deformations. On the other hand, high value of track stiffness leads to increasing dynamic force in the wheel-rail interface as well as on the sleepers and ballast, which can cause wearing and fatigue of track components. Therefore, the use of para rubber as an under sleeper pad is suggested to be the most appropriate method for using in railway track as it is a better solution for decreasing ballast breakage and has only slight influence on track performance on the railway track.

CHAPTER 5
CONCLUSION

5.1 Conclusion

The ballast particle degradation under repeated loads was studied by using the box test. The purposes of this study were to investigate the influences of applying para rubber as a ballast mat and an under-sleeper pad on ballast degradation. The para rubber application was compared with commercial elastic product that was applied as a ballast mat and an under-sleeper pad as well. The ballast rock used in this study was Andesite rock obtained from Vihandaeng in Saraburi province. Five cases of box tests comprised of pure ballast for reference (Ballast Ref.), ballast with a ballast mat using commercial product (Com Mat), ballast with a ballast mat using para rubber (Para Mat), ballast with an under-sleeper pad using commercial product (Com USP), and ballast with an under-sleeper pad using para rubber (Para USP). Each box test was conducted under continuous haversine loading of 5 cycles per second and terminated at 1,000,000 cycles which was equivalent to 20 million tons of axle load passing. On each box test, all ballast particles were weighed and taken their images before and after the test for determining their sizes using image processing and amount of breakage after the test. Based on the objectives of this research, the result of this research can be summarized as follows:

Para rubber and commercial material were used as the ballast mat placed under the ballast layer. Both ballast mat cases had influenced on increasing the ballast degradation comparing to the pure ballast case with the same loading condition. Moreover, both cases could not improve the performance of ballasted track which can be seen from the settlement graphs of both cases of which were higher than the pure ballast case. Likewise, the modulus of the ballast box reaction was lower than the pure ballast case which could be a disadvantage for the ballasted track. The possible influences of these behaviors to the railway track are as follows:

- Significantly higher sleeper settlement may increase the geometric deviation of railway track at a higher rate comparing to a pure ballast case.
- Lowering track modulus will cause increasing of bending stresses in rails. This may shorten the fatigue life of the rails.

Using para rubber and commercial material as USP can decrease the ballast degradation in both coarse breakage and fine breakage from the ballast ref. case. However, the resilient deformation of the Com. USP case was the highest and the modulus of ballast box reaction was the lowest. So, using Com. USP is not appropriate in the ballasted track in the same reasons described earlier. In contrast, Para USP had a better solution. Both sleeper settlement and the modulus of ballast box reaction were close to the ballast ref.

From the results of this study, para rubber can be used appropriately in railway track in the form of under sleeper pad (USP) component. The results indicate that it has ability to reduce ballast degradation and it has minor effects on slightly increasing sleeper settlement and lowering track modulus.

5.2 Limitation of research

In the box test, one million cycles of 20-ton equivalent axle loads at a constant frequency was applied to the five cases. Some railways may experience more severe conditions in load magnitude and number of repetitions. The ballast box test simulated only the ballasted track on the rigid foundation. For a case of ballasted track on flexible foundation e.g. on earth embankment, the output may not be the same. The size of box test only simulate ballast volume underneath a 30-cm portion of sleeper which is subjected to the highest vertical stress by theory. The test did not include environmental factors such as temperature, solar radiation and humidity. The behavior of para rubber under the real environment at the time period of one million repetitions is unknown.

5.3 Recommendation

- It is interesting to conduct the box test at more severe loading conditions including higher load magnitude, different loading frequency, higher number of load repetitions. In addition, a box test that can simulate a flexible foundation shall be explored.
- Ballast and para rubber could be tested in environmental conditions similar to the field including temperature, solar radiation and humidity to observe its performance over a long termed period.
- Other factors of para rubber can be explored including thickness and layout patterns of the pad to find the optimum performance.

REFERENCES

AREMA. (2011). "American Railway Engineering and Maintenance-of-Way Association".

Aursudkij, B., McDowell, G., and Collop, A. (2009). "Cyclic loading of railway ballast under triaxial conditions and in a railway test facility". Granular Matter, 11(6), 391.

Cuelho, E., Mokwa, R., Obert, K., and Miller, A. (2008). Comparative analysis of micro-Deval, LA abrasion, and sulfate soundness tests. Retrieved from

D'Angelo, G., Thom, N., and Presti, D. L. (2015). "Laboratory simulation of field loading conditions and maintenance operations". Proceeding of Railway Engineering.

Du Plooy, R. F., and Gräbe, P. (2017). "Characterisation of rigid polyurethane foam-reinforced ballast through cyclic loading box tests". Journal of the South African Institution of Civil Engineering, 59(2), 2-10.

Ebrahimi, A., Tinjum, J. M., and Edil, T. B. (2010). Large-Scale, cyclic triaxial testing of rail ballast. Paper presented at the AREMA Annual Conference e Exposition, Orlando.

Esmaeili, M., Aela, P., and Hosseini, A. (2017). "Experimental assessment of cyclic behavior of sand-fouled ballast mixed with tire derived aggregates". Soil Dynamics and Earthquake Engineering, 98, 1-11. doi:https://doi.org/10.1016/j.soildyn.2017.03.033

Esveld, C. (2014). Modern railway track. Netherland: MRT-Productions.

Fathali, M., Nejad, F. M., and Esmaeili, M. (2016). "Influence of tire-derived aggregates on the properties of railway ballast material". Journal of Materials in Civil Engineering, 29(1), 04016177.

Getzner. (2015). Sleeper Padding for Ballasted Track

Gupta, A. K. (2009). "Effect of particle size and confining pressure on breakage and strength parameters of rockfill materials". Electronic Journal of Geotechnical Engineering, 14(Bund. H), 1-12.

Ho, C., Humphrey, D., Hyslip, J., and Moorhead, W. (2013). "Use of Recycled Tire Rubber to Modify Track-Substructure Interaction". Transportation Research Record: Journal of the Transportation Research Board(2374), 119-125.

Hunt, H., and WINKLER. (1997). SETTLEMENT OF RAILWAY TRACK NEAR BRIDGE ABUTMENTS.(THIRD PAPER IN YOUNG RAILWAY ENGINEER OF THE YEAR (1996) AWARD). Paper presented at the Proceedings of the Institution of Civil Engineers-Transport.

Indraratna, B., Khabbaz, H., Salim, W., and Christie, D. (2006). "Geotechnical properties of ballast and the role of geosynthetics". Institution of Civil Engineers. Proceedings. Ground...

Indraratna, B., Lackenby, J., and Christie, D. (2005). "Effect of confining pressure on the degradation of ballast under cyclic loading".

Indraratna, B., Salim, W., and Rujikiatkamjorn, C. (2011). Advanced rail geotechnology–ballasted track: CRC press.

Kaewunruen, S., and Remennikov, A. M. (2015). "Under sleeper pads: field investigation of their role in detrimental impact mitigation".

Kashani, H. F., Hyslip, J. P., and Ho, C. L. (2017). "Laboratory evaluation of railroad ballast behavior under heavy axle load and high traffic conditions". Transportation Geotechnics, 11, 69-81.

Kennedy, J. (2011). A full-scale laboratory investigation into railway track substructure performance and ballast reinforcement. Heriot-Watt University.

Koike, Y., Nakamura, T., Hayano, K., and Momoya, Y. (2014). "Numerical method for evaluating the lateral resistance of sleepers in ballasted tracks". Soils and Foundations, 54(3), 502-514.

Koohmishi, M., and Palassi, M. (2018). "Degradation of railway ballast under compressive loads considering particles rearrangement". International Journal of Pavement Engineering, 1-13.

Kwan, A. K., Mora, C., and Chan, H. (1999). "Particle shape analysis of coarse aggregate using digital image processing". Cement and Concrete Research, 29(9), 1403-1410.

Lade, P. V., Yamamuro, J. A., and Bopp, P. A. (1996). "Significance of particle crushing in granular materials". Journal of Geotechnical Engineering, 122(4), 309-316.

Lee, K. L., and Farhoomand, I. (1967). "Compressibility and crushing of granular soil in anisotropic triaxial compression". Canadian geotechnical journal, 4(1), 68-86.

Liu, S., Huang, H., Qiu, T., and Kwon, J. (2016). "Effect of geogrid on railroad ballast particle movement". Transportation Geotechnics, 9, 110-122. doi:https://doi.org/10.1016/j.trgeo.2016.08.003

Lundqvist, A., and Dahlberg, T. (2005). Railway track stiffness variation-consequences and countermeasures. Paper presented at the 19th IAVSD Symposium of Dynamics of Vehicles on Roads and Tracks, Milano, August 29-Seprember 2, 2005.

Marsal, R. J. (1967). "Large-scale testing of rockfill materials". Journal of the Soil Mechanics and Foundations Division, 93(2), 27-43.

Navaratnarajah, S. K., and Indraratna, B. (2017). "Use of rubber mats to improve the deformation and degradation behavior of rail ballast under cyclic loading". Journal of geotechnical and geoenvironmental engineering, 143(6), 04017015.

Qian, Y., Boler, H., Moaveni, M., Tutumluer, E., Hashash, Y., and Ghaboussi, J. (2014). "Characterizing ballast degradation through Los Angeles abrasion test and image analysis". Transportation Research Record: Journal of the Transportation Research Board(2448), 142-151.

Qian, Y., Mishra, D., Tutumluer, E., and Kazmee, H. A. (2015). "Characterization of geogrid reinforced ballast behavior at different levels of degradation through triaxial shear strength test and discrete element modeling". Geotextiles and Geomembranes, 43(5), 393-402. doi:https://doi.org/10.1016/j.geotexmem.2015.04.012

Raymond, G. P. (2002). "Reinforced ballast behaviour subjected to repeated load". Geotextiles and Geomembranes, 20(1), 39-61.

Retrieved from https://www.getzner.com/en/products/rail-products/sleeper-pads

Salim, W. (2004). "Deformation and degradation aspects of ballast and constitutive modelling under cyclic loading".

Selig, E. T., and Waters, J. M. (1994). Track geotechnology and substructure management: Thomas Telford.

Shenton, M. (1978). Deformation of railway ballast under repeated loading conditions Railroad track mechanics and technology (pp. 405-425): Elsevier.

Sol-Sánchez, M., Moreno-Navarro, F., and Rubio-Gámez, M. (2014). "The use of deconstructed tires as elastic elements in railway tracks". Materials, 7(8), 5903-5919.

Sol-Sánchez, M., Moreno-Navarro, F., and Rubio-Gámez, M. C. (2015). "The use of elastic elements in railway tracks: A state of the art review". Construction and Building Materials, 75, 293-305.

Sol-Sánchez, M., Thom, N. H., Moreno-Navarro, F., Rubio-Gámez, M. C., and Airey, G. D. (2015). "A study into the use of crumb rubber in railway ballast". Construction and Building Materials, 75, 19-24. doi:https://doi.org/10.1016/j.conbuildmat.2014.10.045

Suku, L., Prabhu, S. S., Ramesh, P., and Babu, G. L. S. (2016). "Behavior of geocell-reinforced granular base under repeated loading". Transportation Geotechnics, 9, 17-30. doi:https://doi.org/10.1016/j.trgeo.2016.06.002

Sun, Q., Indraratna, B., and Nimbalkar, S. (2014). "Effect of cyclic loading frequency on the permanent deformation and degradation of railway ballast". Géotechnique.

Vadood, M., Johari, M. S., and Rahaei, A. R. (2014). "Introducing a simple method to determine aggregate gradation of hot mix asphalt using image processing". International Journal of Pavement Engineering, 15(2), 142-150.

Vanicek, I., and Vanicek, M. (2008). Earth structures: in transport, water and environmental engineering (Vol. 4): Springer Science & Business Media.

Zakeri, J. A. (2012). Lateral resistance of railway track Reliability and safety in railway: InTech.

จุฬาลงกรณ์มหาวิทยาลัย

CHULALONGKORN UNIVERSITY

APENDICT

(Example of top view photo and side view photo)

(Example of image processing analysis)
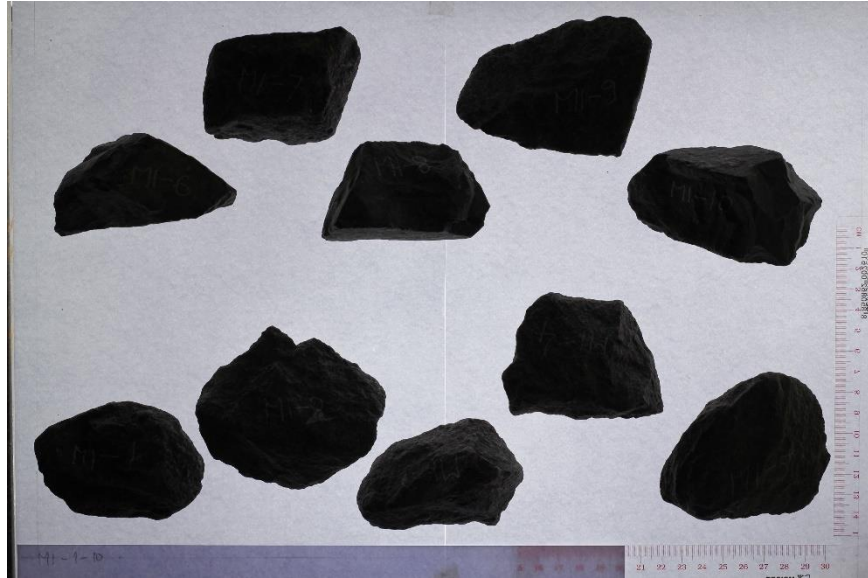
(Example of the image processing result)

No particle	Area	XM	YM	Feret	FeretX	FeretY	FeretAngle	MinFeret
1	2678.551	69.768	226.683	66.459	37.236	220.324	168.14	53.494
2	1773.686	150.019	200.64	61.76	124.959	193.17	162.376	44.712
3	2306.441	215.469	234.021	64.481	183.17	241.219	10.828	47.441
4	2503.326	271.724	188.48	68.748	239.186	175.121	167.64	48.456
5	2831.164	347.965	224.543	77.497	310.568	221.544	13.468	59.628
6	4753.815	82.786	127.887	100.872	30.325	146.991	32.191	69.559
7	2447.579	144.686	54.367	70.831	111.544	36.829	149.284	49.241
8	2508.799	206.011	117.436	75.856	171.463	133.008	14.081	46.728
9	3552.786	305.96	65.491	96.065	264.308	88.048	27.194	48.067
10	2381.316	358.98	124.141	79.247	319.186	139.43	20.164	47.618
1	3746.905	73.337	232.129	97.608	27.811	246.08	16.207	53.34
2	2209.467	138.42	187.598	71.027	104.432	192.972	19.055	44.492
3	2136.692	191.64	215.409	61.539	161.837	215.837	147.482	43.922
4	3086.747	268.765	206.462	84.111	227.513	206.756	178.453	56.489
5	3150.562	348.587	229.146	71.265	314.35	242.188	6.664	60.026
6	2061.708	70.726	59.404	62.365	44.919	49.621	157.77	48.811
7	2105.715	133.952	115.517	60.257	105.729	102.973	158.614	47.483
8	4187.086	204.554	60.403	84.02	162.162	74.27	177.179	71.073
9	5468.246	282.927	121.875	109.399	235.053	113.513	174.94	77.189
10	2123.215	340.399	57.131	66.36	307.62	55.459	162.141	50.235
1	2003.151	74.654	227.96	61.492	41.626	230.487	24.362	50.705
2	3658.046	162.858	185.288	80.865	133.414	213.17	46.711	62.263
3	2418.881	232.947	238.712	89.253	190.731	239.268	176.71	34.044
4	2232.498	293.751	186.567	65.632	258.943	182.195	171.308	45.255
5	1693.833	350.45	230.887	55.554	326.991	243.333	29.454	39.599
6	2057.114	62.094	122.547	68.859	23.821	120.569	160.624	47.629
7	2230.132	129.148	63.685	69.369	95.122	55.366	6.933	45.399
8	3594.611	198.61	117.274	90.395	151.951	123.17	8.378	54.724
9	3721.215	290.512	62.619	85.888	249.999	55.284	159.73	61.996
10	2134.323	349.838	118.057	59.847	326.178	97.154	153.539	49.307
1	3250.353	64.815	234.34	86.496	18.862	238.943	174.498	50.022
2	1579.754	136.45	210.652	53.964	112.032	201.463	159.818	39.405
3	2695.184	196.379	239.668	67.574	165.203	244.146	6.98	52.293
4	2941.134	279.339	225.472	88.339	239.186	221.544	175.355	48.982
5	1516.908	366.05	243.441	56.099	335.446	239.756	163.325	38.935
6	1539.97	54.116	174.936	51.926	30.325	156.585	136.332	42.331
7	1433.175	132.395	156.475	58.621	105.366	144.065	149.772	37.593
8	1840.484	202.869	157.827	67.284	166.016	158.618	9.178	43.435
9	2197.4	276.276	158.34	63.607	246.666	152.114	161.982	51.477
10	2963.938	355.761	153.886	79.257	321.381	139.349	165.08	49.31
11	2451.044	47.141	116.216	72.29	15.203	100.244	152.542	52.045
12	2907.609	134.674	104.205	86.927	89.268	100.975	169.71	49.755
13	1921.666	220.67	101.968	68.591	188.211	110.894	21.12	36.859
14	1652.634	293.458	99.701	63.963	262.926	85.528	154.314	39.201
15	1130.85	369.022	100.12	49.671	344.227	109.024	14.309	26.434
16	4009.389	56.686	45.919	81.388	14.553	49.837	24.491	68.804
17	1866.738	137.02	41.738	56.459	110	37.886	170.049	45.873
18	1564.796	203.018	41.019	56.418	181.626	18.049	131.963	43.284
19	1849.05	274.243	38.764	55.761	249.918	49.268	23.912	45.184
20	2993.391	364.112	42.609	82.052	318.78	33.821	157.144	59.281

Table of Ballast degradation.						
Sample	weight before test (g)	weight after test (g)	Coarse breakage (g)	fine weight (g)	Fine Breakage %	Coarse breakage %
Ballast ref	89521.03	89193.5	300.302	27.23	0.030417	0.335454
Para mat	89799.45	89333.43	413.332	52.69	0.058675	0.460283
Com. Mat	90231.26	89726.98	408.88	95.4	0.105728	0.453147
Para USP	89982.62	89913.53	46.71	22.38	0.024871	0.05191
Com. USP	90520.74	90334.3	125.63	60.81	0.067178	0.138786

Table of ballast breakage at different location in the box				
Zone	Mass Before Test (g)	Mass After Test (g)	Mass Before-After Test (g)	Percent weight loss (%)
L1	14545.53	14524.93	20.60	0.0230
L2	14875.76	14870.04	5.72	0.0064
M1	15184.662	15160.91	23.75	0.0265
M2	14874.51	14747.11	127.40	0.1423
R1	14996.81	14854.85	141.96	0.1586
R2	15043.76	15035.66	8.10	0.0090

Table the distribute of ballast particle size					
SIZE (mm)	Ballast ref	Para mat	Com. Mat	Para USP	Com. USP
0-15	0	0	0	0	0
15-20	0	0	0	0	0
20-25	0	7	2	4	2
25-30	25	34	18	30	44
30-35	65	115	83	101	109
35-40	109	104	124	121	141
40-45	143	153	152	126	142
45-50	144	140	119	126	137
50-55	104	103	115	124	110
55-60	77	70	67	81	73
60-65	49	50	51	48	55
65-70	29	32	37	32	20
70-75	16	11	11	7	16
75-80	6	6	5	1	3
80-85	2	1	1	2	2
More	0	0	0	0	0

Table Number of ballast breakage at difference weight loss				
weight (g)	Ballast ref	Para mat	Com. Mat	Para USP	Com. USP
0-0.05	536	506	523	377	357
0.05-0.1	164	163	114	105	300
0.1-0.15	29	49	43	22	90
0.15-0.2	8	21	17	11	35
0.2-0.25	6	14	9	1	15
0.25-0.3	1	5	8	1	10
0.3-0.35	1	8	5	3	6
0.35-0.4	4	4	6	3	5
0.4-0.45	3	7	5	2	2
0.45-0.5	2	2	4	2	1
0.5-0.55	2	3	3	2	2
0.55-0.6	0	3	5	1	3
0.6-0.65	0	1	4	1	1
0.65-0.7	1	1	0	1	0
0.7-0.75	0	2	0	0	2
0.75-0.8	0	0	2	0	0
0.8-0.85	0	4	2	0	2
0.85-0.9	0	2	2	0	1
0.9-0.95	0	1	1	0	2
0.95-1	0	3	0	0	0
More	13	27	32	2	20

Example of percent weight change of a [particle in each size				
Max minor	Mass (g) Before test	Mass (g) After test	weight change	%weight change
53.494	75.94	75.92	0.02	0.02633658
44.712	82.49	82.48	0.01	0.01212268
47.441	105.85	105.79	0.06	0.05668399
48.456	61.07	61.02	0.05	0.08187326
59.628	126.24	126.16	0.08	0.06337136
69.559	284.29	284.18	0.11	0.03869288
49.241	60.43	60.39	0.04	0.06619229
46.728	138.54	138.5	0.04	0.02887253
48.067	222.21	222.19	0.02	0.0090005
47.618	159.33	159.25	0.08	0.05021026
53.34	202.97	202.89	0.08	0.03941469
44.492	129.64	129.58	0.06	0.04628201
43.922	108.75	108.73	0.02	0.0183908
56.489	136.84	136.73	0.11	0.08038585
60.026	152.1	152.09	0.01	0.00657462
48.811	137.21	137.18	0.03	0.0218643
47.483	130.34	130.26	0.08	0.06137793
71.073	223.28	223.19	0.09	0.04030813
77.189	298.79	298.76	0.03	0.0100405
50.235	127.12	127.08	0.04	0.03146633
50.705	129.23	129.18	0.05	0.03869071
62.263	154.62	154.57	0.05	0.03233734
34.044	122.55	122.52	0.03	0.0244798
45.255	83.72	83.69	0.03	0.03583373
39.599	47.73	47.7	0.03	0.06285355
47.629	88.49	88.44	0.05	0.05650356
45.399	119.5	119.45	0.05	0.041841
54.724	212.4	212.31	0.09	0.04237288
61.996	177.81	177.76	0.05	0.0281199
49.307	102.15	102.13	0.02	0.01957905
50.022	166.43	166.35	0.08	0.04806826
39.405	52.76	52.73	0.03	0.05686126
52.293	79.47	79.46	0.01	0.01258336
48.982	143.68	143.61	0.07	0.04871938
38.935	41.81	41.8	0.01	0.02391772
42.331	68.7	68.69	0.01	0.01455604
37.593	62.71	62.67	0.04	0.06378568
43.435	57.04	57.02	0.02	0.03506311
51.477	96.6	96.54	0.06	0.0621118
49.31	111.35	111.33	0.02	0.01796138
52.045	78.2	78.16	0.04	0.0511509
49.755	193.29	193.25	0.04	0.02069429
36.859	61.09	61	0.09	0.14732362
39.201	80.54	80.52	0.02	0.02483238
26.434	60.55	60.53	0.02	0.03303055
68.804	202.02	201.96	0.06	0.02970003
45.873	57.84	57.82	0.02	0.03457815
43.284	55.31	55.28	0.03	0.05423974

Table of the distribution of percent weight loss in each size					
size	Ballast ref	Para Mat	Com.Mat	Para USP	Com. USP
0-20	0	0	0	0	0
20-25	0	1.22	0.04	0.07	0.01
25-30	0.35	0.79	9.08	0.64	3.37
30-35	17.05	93.792	44.32	3.76	8.29
35-40	4.46	84.08	59.4	25.86	17.09
40-45	23.2	43.29	12.14	5.21	34.47
45-50	6.66	34.88	102.85	6.35	10.68
50-55	214.44	13.14	90.18	6.2	76.15
55-60	7.59	100.63	12.21	15.36	21.18
60-65	16.942	6.76	122.43	2.81	9.09
65-70	34.01	6.86	3.45	1.81	2.29
70-75	1.51	2.89	47.67	0.87	2.07
75-80	0.55	77.62	0.51	0.01	0.41
80-85	0.77	0.07	0	0.14	1.34
more	0	0	0	0	0

Table Distribution of ballast in each L/W ratio of all samples					
L/W	Ballast ref	Para mat	Com. Mat	Para USP	Com. USP
0.75-1	0	0	0	0	0
1-1.25	109	135	104	118	136
1.25-1.5	371	358	364	361	366
1.5-1.75	197	214	171	200	213
1.75-2	63	81	94	84	92
2-2.25	22	26	31	24	30
2.25-2.5	4	6	13	12	11
2.5-2.75	4	6	5	2	5
2.75-3	0	0	2	2	1
More	0	0	1	0	0

Table Percent frequency ballast breakage by weight loss in each L/W ratio					
L/W	Ballast ref	Para Mat	Com.Mat	Para USP	Com. USP
0.75-1	0.00	0.00	0.00	0.00	0.00
1-1.25	0.02	0.22	0.12	0.00	0.01
1.25-1.5	0.07	0.17	0.17	0.04	0.08
1.5-1.75	0.06	0.10	0.16	0.02	0.09
1.75-2	0.07	0.03	0.06	0.01	0.02
2-2.25	0.14	0.00	0.04	0.00	0.01
2.25-2.5	0.00	0.00	0.00	0.00	0.00
2.5-2.75	0.00	0.00	0.00	0.00	0.00
2.75-3	0.00	0.00	0.00	0.00	0.00

Table particle weight loss by L/W ratio					
L/W	Ballast ref	Para Mat	Com.Mat	Para USP	Com. USP
1-1.25	0.192	1.521	1.038	0.037	0.091
1.25-1.5	0.153	0.393	0.370	0.095	0.185
1.5-1.75	0.200	0.354	0.763	0.083	0.368
1.75-2	0.798	0.252	0.490	0.056	0.137
2-2.25	3.672	0.128	0.754	0.063	0.163
2.25-2.5	0.027	0.267	0.029	0.029	0.060
2.5-2.75	0.048	0.056	0.027	0.051	0.044
2.75-3	0.000	0.000	0.367	0.045	0.066

Table distribution of ballast in each H/W ratio of all samples					
H/W	Ballast ref	Para mat	Com. Mat	Para USP	Com. USP
0-0.2	0	1	0	0	0
0.2-0.3	4	6	3	7	6
0.3-0.4	20	49	31	27	43
0.4-0.5	74	85	74	77	104
0.5-0.6	154	152	163	138	155
0.6-0.7	196	172	188	184	185
0.7-0.8	186	174	158	180	178
0.8-0.9	86	98	126	111	108
0.9-1	50	89	42	79	75
More	0	0	0	0	0

Table Percent total weight loss in each H/W ratio					
H/W	Ballast ref (%)	Para Mat (%)	Com.Mat (%)	Para USP (%)	Com. USP (%)
0.2-0.3	0.0002	0.0006	0.0001	0.0005	0.0132
0.3-0.4	0.0013	0.0460	0.0037	0.0018	0.0149
0.4-0.5	0.0044	0.1197	0.1099	0.0047	0.0197
0.5-0.6	0.0603	0.1415	0.1544	0.0079	0.0332
0.6-0.7	0.1553	0.1618	0.1271	0.0092	0.0320
0.7-0.8	0.0128	0.0129	0.0301	0.0447	0.0164
0.8-0.9	0.0045	0.0272	0.0358	0.0047	0.0681
0.9-1	0.1272	0.0092	0.0980	0.0033	0.0085
more	0.0000	0.0000	0.0000	0.0000	0.0000

Table percent particle weight loss by ballast H/W ratio					
H/W	Ballast ref	Para Mat	Com.Mat	Para USP	Com. USP
0.2-0.3	0.000	1.831	0.000	0.000	0.000
0.3-0.4	0.000	15.466	1.694	0.319	4.447
0.4-0.5	0.207	2.961	2.983	0.164	0.667
0.5-0.6	0.656	1.694	1.757	0.087	0.287
0.6-0.7	0.748	0.823	0.608	0.048	0.186
0.7-0.8	0.048	0.057	0.118	0.199	0.064
0.8-0.9	0.018	0.118	0.172	0.020	0.310
0.9-1	1.132	0.077	0.621	0.024	0.070

Table distribution of ballast particle in each H/L					
H/L	Ballast ref	Para Mat	Com.Mat	Para USP	Com. USP
0.1-0.2	2	5	3	5	7
0.2-0.3	45	87	69	65	79
0.3-0.4	179	196	200	166	218
0.4-0.5	291	241	254	257	273
0.5-0.6	172	190	179	219	187
0.6-0.7	68	78	71	74	77
0.7-0.8	12	24	9	16	12
0.8-0.9	1	5	0	1	1
0.9-1	0	0	0	0	0

Table Percent total eight loss by ballast H/L ratio					
H/L	Ballast ref	Para Mat	Com.Mat	Para USP	Com. USP
0.1-0.2	0.0001	0.0006	0.0003	0.0000	0.0132
0.2-0.3	0.0199	0.0760	0.0083	0.0001	0.0228
0.3-0.4	0.1214	0.1644	0.2631	0.0001	0.0350
0.4-0.5	0.1945	0.1277	0.1164	0.0002	0.0507
0.5-0.6	0.0270	0.1225	0.1425	0.0001	0.0751
0.6-0.7	0.0027	0.0263	0.0130	0.0003	0.0084
0.7-0.8	0.0002	0.0012	0.0153	0.0000	0.0007
0.8-0.9	0.0000	0.0000	0.0000	0.0000	0.0000

Table percent particle weight loss by H/L ratio					
H/L	Ballast ref	Para Mat	Com.Mat	Para USP	Com. USP
0.1-0.2	0.099	0.188	0.059	0.075	2.775
0.2-0.3	0.347	0.970	0.096	0.058	0.271
0.3-0.4	0.497	0.661	0.967	0.050	0.136
0.4-0.5	0.479	0.398	0.359	0.074	0.156
0.5-0.6	0.133	0.534	0.638	0.035	0.321
0.6-0.7	0.036	0.307	0.160	0.321	0.103
0.7-0.8	0.015	0.040	1.901	0.036	0.054
0.8-0.9	0	0	0	0	0

Example of data from cyclic test				
Cycle count	TD1 kN Upper value	TD1 kN Lower value	TD2 mm Upper value	TD2 mm Lower value
1	-13.48669338	-13.72098637	19.93732071	19.93328476
100	-0.367904991	-28.00232506	20.28311539	19.76421928
200	-0.394225001	-27.98411942	20.28033066	19.76373672
300	-0.426138997	-28.05517578	20.27729988	19.76295471
400	-0.393070012	-27.90070534	20.27954674	19.76423264
500	-0.396643013	-28.05426216	20.27802658	19.76275253
600	-0.395687014	-27.90770149	20.27848816	19.76430511
700	-0.464116007	-27.91927528	20.27322006	19.76403809
800	-0.463277012	-27.88095474	20.2723732	19.76453972
900	-0.434763998	-27.88988686	20.27372551	19.76389885
1000	-0.451332986	-27.99729156	20.27351761	19.76342964
1100	-0.431531012	-28.09989738	20.27466965	19.76200867
1200	-0.412658006	-28.0653553	20.27546883	19.76235008
1300	-0.402251989	-28.0236454	20.27603531	19.76239586
1400	-0.469610006	-28.15921593	20.27142143	19.76115036
1500	-0.385901988	-28.02519417	20.27634811	19.76235962
1600	-0.349164993	-27.85920334	20.27809715	19.76398277
1700	-0.34799099	-27.81040192	20.27807808	19.76400566
1800	-0.42474699	-28.15539932	20.27423668	19.76090431
1900	-0.427973002	-28.14639664	20.27341461	19.76110649
2000	-0.379961014	-27.95939827	20.27625847	19.76299286
2500	-0.386514008	-27.9960022	20.27388573	19.76212883
3000	-0.427706003	-27.93592072	20.27202797	19.76299667
3500	-0.420062989	-28.02918625	20.27252388	19.76165009
4000	-0.406378001	-28.11585236	20.27290344	19.76005745
4500	-0.414258003	-27.87700081	20.27207947	19.76234245
5000	-0.419283003	-28.07131767	20.27096176	19.76074219
5500	-0.401753992	-27.92118263	20.27161026	19.7617054
6000	-0.359872997	-28.04340553	20.27474785	19.76063728
6500	-0.437723011	-28.07581711	20.27069092	19.75975037
7000	-0.422659993	-27.79284286	20.27120209	19.76174164
7500	-0.428689986	-27.78440285	20.27051735	19.76106453
8000	-0.390924007	-28.09812355	20.27319908	19.75869751
8500	-0.430485994	-27.90498924	20.27058792	19.76015091
9000	-0.458324999	-27.93123055	20.26984978	19.7600441
9500	-0.38132	-28.15049171	20.27393341	19.75816917

Example of data colected in one cycle from cyclic test			
Cycle	Time	TD1 kN	TD2 mm
1	0	-13.490889	19.9370518
1	2.00E-03	-13.506877	19.9369125
1	4.00E-03	-13.497436	19.9372101
1	6.00E-03	-13.497265	19.9365921
1	8.00E-03	-13.50518	19.9368057
1	1.00E-02	-13.512094	19.9366627
1	1.20E-02	-13.497334	19.9367237
1	1.40E-02	-13.509208	19.9364872
1	1.60E-02	-13.51936	19.936264
1	1.80E-02	-13.511457	19.9367561
1	0.02	-13.511009	19.9364643
1	2.20E-02	-13.529647	19.9360332
1	2.40E-02	-13.515806	19.9361935
1	2.60E-02	-13.521194	19.9358215
1	2.80E-02	-13.528057	19.935854
1	3.00E-02	-13.530268	19.9361916
1	3.20E-02	-13.51707	19.9358139
1	3.40E-02	-13.528234	19.9362202
1	3.60E-02	-13.533405	19.9363136
1	3.80E-02	-13.535231	19.9359684
1	4.00E-02	-13.529527	19.9359436
1	0.042	-13.548877	19.9360561
1	4.40E-02	-13.53805	19.9361687
1	4.60E-02	-13.534102	19.9354038
1	4.80E-02	-13.544708	19.9358177
1	5.00E-02	-13.55594	19.9358177
1	5.20E-02	-13.532482	19.9359665
1	5.40E-02	-13.553489	19.9357052
1	5.60E-02	-13.553007	19.9358921
1	5.80E-02	-13.546622	19.9361382
1	6.00E-02	-13.552725	19.9355869
1	0.062	-13.569631	19.9353275
1	6.40E-02	-13.555428	19.9355679
1	6.60E-02	-13.555248	19.9358425
1	6.80E-02	-13.559109	19.9358959
1	7.00E-02	-13.561179	19.9356136
1	7.20E-02	-13.552392	19.9355125
1	7.40E-02	-13.564156	19.9353752
1	7.60E-02	-13.565923	19.9355087
1	7.80E-02	-13.561866	19.9361115
1	8.00E-02	-13.554657	19.9355831
1	0.082	-13.578715	19.9353695
1	8.40E-02	-13.567762	19.9355106
1	8.60E-02	-13.565428	19.9354973
1	8.80E-02	-13.57744	19.9358692
1	9.00E-02	-13.578566	19.9352322
1	9.20E-02	-13.558598	19.9355049
1	9.40E-02	-13.576843	19.9350948
1	9.60E-02	-13.578393	19.9353161

VITA

NAME   Somkith Dethvongsone

DATE OF BIRTH   19 April 1993

PLACE OF BIRTH   Savannakhet Province, LAO PDR

INSTITUTIONS   I graduated the high school level in in the academic year
ATTENDED   2012 at Vientiane High School, Vientiane Province, Lao
                            PDR. I was graduated the Bachelor's degree at the
                            National University of Laos In academic year 2016, my
                            major is civil engineering and I have attended to study in
                            Master's degree in the academic year 2016 at Civil
                            Engineering Department, Faculty of Engineering,
                            Chulalongkorn University, Thailand
HOME ADDRESS   Road Number 9, Zay Tharmuak village, Phin district,
                            Savannakhet province, LAO PDR.